

Tailoring properties of borohydrides for hydrogen storage: A review

Feature Article

Line H. Rude¹, Thomas K. Nielsen², Dorthe B. Ravnsbæk¹, Ulrike Bösenberg³, Morten B. Ley¹, Bo Richter¹, Lene M. Arnbjerg¹, Martin Dornheim³, Yaroslav Filinchuk^{4,5}, Flemming Besenbacher⁶, and Torben R. Jensen^{*,1,2}

¹Center for Materials Crystallography, Interdisciplinary Nanoscience Center and Department of Chemistry, Aarhus University, Langelandsgade 140, 8000 Århus C, Denmark

²Center for Energy Materials, Interdisciplinary Nanoscience Center and Department of Chemistry, Aarhus University, Langelandsgade 140, 8000 Århus C, Denmark

³Institute of Materials Research, Materials Technology, Helmholtz-Zentrum Geesthacht, 21502 Geesthacht, Germany

⁴Swiss-Norwegian Beam Lines at ESRF, BP-220, 38043 Grenoble, France

⁵Institute of Condensed Matter and Nanosciences, Université Catholique de Louvain, Place L. Pasteur 1, 1348 Louvain-la-Neuve, Belgium

⁶Center for Energy Materials, Interdisciplinary Nanoscience Center (iNANO) and Department of Physics and Astronomy, Aarhus University, 8000 Århus C, Denmark

Received 12 November 2010, revised 21 February 2011, accepted 21 February 2011

Published online 13 July 2011

Keywords anion substitution, hydrogen storage, metal borohydrides, nano confinement, reactive hydride composites

* Corresponding author: e-mail trj@chem.au.dk, Phone: +45 8942 3894, Fax: +45 8619 6199

Hydrogen is recognized as a possible future energy carrier, which can be produced from renewable energy and water. A major challenge in a future ‘hydrogen economy’ is the development of safe, compact, robust, and efficient means of hydrogen storage, in particular for mobile applications. The present review focuses on light metal boron based hydrides, for which the general interest has expanded significantly during the past few years. Synthesis methods, physical, chemical and structural properties of novel boron based hydrides are

reviewed along with new approaches for improving kinetic and thermodynamic properties: (i) anion substitution, (ii) reactive hydride composites and (iii) nanoconfinement of hydrides and chemical reactions. The light metal borohydrides reveal a fascinating structural chemistry and have the potential for storing large amounts of hydrogen. A combination of the different approaches may provide a new route to a wide range of interesting energy storage materials in the future.

© 2011 WILEY-VCH Verlag GmbH & Co. KGaA, Weinheim

1 Introduction Fossil fuels form the fundament for the development of the industrialized world, initiated in 1769 by James Watt’s patent of the steam engine. Since then, the world energy consumption has been increasing nearly exponentially, and forecasts predict it will be doubled from 2007 to 2035 partly due to the rapidly growing human population on the globe [1]. A close correlation exists between energy availability and prices and the economical growth and stability in the industrialized world. The industrialized world strongly depends on unlimited and cheap energy, which in the past century has been available in the form of fossil fuels, i.e. oil, gas and coal. A large fraction of the available fossil fuels has been consumed during the past 100 years and a major fraction of the remaining reserves

will likely be consumed during the coming decades [1–5]. The consumption of fossil fuels has led to rapidly increasing levels of carbon dioxide CO₂ in the atmosphere, and it is now widely accepted that this may give rise to an increase in the average temperature on earth and to climatic changes. However, the exact climate response to the increasing levels of CO₂ still remains unknown [6].

The transition towards a sustainable, carbon-free and reliable energy system capable of meeting the increasing energy demands is considered one of the greatest challenges in the 21st century. An obvious alternative to fossil fuels is the use of renewable energy sources, e.g. sun-, wind-, water-, wave- or geothermal-energy, which can generate either heat or electricity [7, 8]. However, one of the major obstacles is

that these renewable energy sources are unevenly distributed both over time and geographically. Most countries will need to integrate several different energy sources and an advanced energy storage system needs to be developed.

Hydrogen has an extreme potential as an energy carrier [9–12]. Hydrogen can be produced from renewable energy sources by electrolytic water splitting, however, a major challenge in a future ‘hydrogen economy’ is the development of safe, compact, robust and efficient means of hydrogen storage, in particular for mobile applications [13]. Hydrogen, the lightest element, has a large gravimetric energy density of 120 MJ/kg, which is, approximately three times higher than that of gasoline. On the other hand, the volumetric energy density of hydrogen is low due to a low density both in gaseous and liquid state of only 0.089 and 71 g/L, at 25 and $-252\text{ }^{\circ}\text{C}$, respectively. Therefore, physical storage of hydrogen as a gas or liquid provide a limited energy content and a more dense storage of hydrogen remains a major obstacle in order to create an efficient ‘hydrogen-society’ [9, 13]. Solid state hydrogen storage has the potential to reach significantly higher hydrogen storage capacities than the storage of hydrogen in the gas or liquid state [13–16].

The abundant and cheap metal, magnesium was investigated due to a decent gravimetric hydrogen storage density MgH_2 of $\rho_{\text{m}}(\text{H}_2) = 7.6\text{ wt}\%$. Unfortunately, due to unfavourable thermodynamic properties, $\Delta H_{\text{f}} = 75\text{ kJ/mol H}_2$, bulk MgH_2 must be heated to $\sim 300\text{ }^{\circ}\text{C}$ in order to release hydrogen at $p(\text{H}_2) = 1\text{ bar}$ [17]. However, significant improvements in kinetic and/or thermodynamic properties can be achieved by ball milling Mg/MgH_2 with additives like V_2O_5 or Nb_2O_5 or by alloying the system with, e.g. Ti, Fe, Ni, Cu or Al [18–28]. This may allow practical utilization under more moderate conditions. Experimental studies have shown increased desorption pressures for nanoparticles ($\sim 5\text{ nm}$) and nanoconfinement has been shown to improve the stability during reversible hydrogen release and uptake, kinetics, and possibly also the thermodynamic properties of chemical reactions involved in reversible release and uptake of hydrogen [17, 29–32].

Covalently bonded hydrogen in complex aluminium and boron-based hydrides has been revisited during the past decade for consideration as possible hydrogen storage materials. A breakthrough was the discovery that hydrogen release and uptake from sodium alanate, NaAlH_4 , can be catalysed by titanium compounds [33, 34]. One of the most frequently used additives is TiCl_3 but other d- and f-block metals have similar properties.

The light element borohydrides have received significant attention during the past few years due to their extremely high hydrogen contents, e.g. lithium borohydride, LiBH_4 , has a hydrogen content of $\rho_{\text{m}} = 18.5\text{ wt}\%$ and $\rho_{\text{v}} = 122.5\text{ kg H}_2/\text{m}^3$ [35]. However, the use of LiBH_4 as a solid-state hydrogen storage material is hampered by unfavourable high thermal stability, i.e. hydrogen is released only at temperatures above $\sim 400\text{ }^{\circ}\text{C}$ and uptake of H_2 only occurs under extreme conditions such as $p(\text{H}_2) \sim 70\text{--}350\text{ bar}$ and $T \sim 600\text{--}650\text{ }^{\circ}\text{C}$ and with relatively slow kinetics [11, 16, 18, 36].

A number of different experimental approaches can be applied to improve the storage properties of borohydrides. First of all, new materials can be intelligently designed using the recently revealed empirical relationship between the Pauling electronegativity of the metal cation and the decomposition temperature [37]. A variety of novel borohydrides with fascinating structures, and in some cases also low decomposition temperatures, have recently been synthesized [38, 39]. Furthermore, the storage properties of known borohydrides can be improved by a number of different approaches: (i) Tailoring the physical properties of the hydrogen storage materials by anion substitution is a novel approach of great potential [40, 41]. (ii) The properties of metal hydrides may be improved by chemical reactions as realized in reactive hydride composites (RHC), which may have significantly improved thermodynamic properties as observed, e.g. for the $2\text{LiBH}_4\text{--MgH}_2$ system [42–46]. (iii) Nanoconfinement of the hydrogen storage materials may improve the reversibility, stability, kinetics, and possibly also the thermodynamic properties of chemical reactions involved in reversible release and uptake of hydrogen [29, 30]. In general, the light metal borohydrides reveal fascinating structural chemistry, physical and chemical properties, which are reviewed here, along with their potential for storing large amounts of hydrogen.

2 Synthesis strategies Borohydride materials are in general synthesized by two different techniques: Wet chemistry synthesis (solvent mediated synthesis) or mechano-chemical synthesis (ball milling) [47]. Wet chemistry methods often facilitate synthesis of pure materials, in contrast to mechano-chemical methods where significant amounts of halide salts usually are formed as by-products. However, mechanical milling is convenient and widely used and some products may only be obtained by this technique, e.g. $\text{LiZn}_2(\text{BH}_4)_5$ [48].

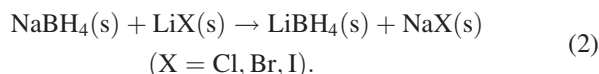
2.1 Solvent-mediated synthesis The first metal borohydride, $\text{Al}(\text{BH}_4)_3$, was synthesized by Schlesinger et al. [49]. An attempt to prepare AlH_3 from trimethyl aluminum and diborane unexpectedly resulted in $\text{Al}(\text{BH}_4)_3$ and trimethylborane. Today, this particular compound is easily synthesized via a quantitative metathesis reaction of aluminum trichloride and LiBH_4 according to reaction scheme (1) [50].



The most commonly encountered and well-known borohydride today is NaBH_4 finding its use in many instances, e.g. as a reducing agent in organic chemistry. Its production has been subject to more than 100 different methods, and the large industrial production scale is underlining the wide variety of applications [51].

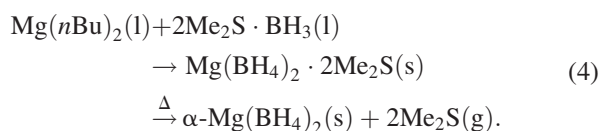
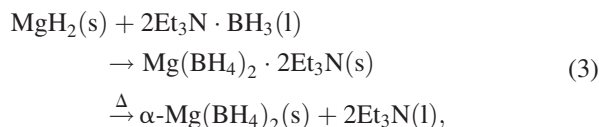
The second most utilized metal borohydride is LiBH_4 , first synthesized from ethyl lithium and diborane by Schlesinger and Brown [52]. It is readily obtained from

NaBH₄ and a lithium halide salt in isopropylamine (IPA) solvent, see reaction scheme (2) [53, 54].



Extraction by diethylether and subsequent removal of the solvent in vacuum yields pure LiBH₄. Today a number of synthesis methods exist, e.g. direct formation from the elements under harsh conditions [55]. Moreover, some borohydrides are stable in basic aqueous solutions and KBH₄ can be produced by a reaction between NaBH₄ and KOH [56]. Alkaline earth borohydrides can be synthesized by a metathesis reaction similar to reaction scheme (1).

Several new synthesis methods of magnesium borohydride, Mg(BH₄)₂, have been developed attempting to yield phase pure, solvent free products. The first successful synthesis was accomplished by Wiberg and Bauer [57] by reaction between diethylmagnesium (MgEt₂) and diborane in ether. Two reliable routes rely on either the reaction between MgH₂ and triethylamineborane complex [58] at elevated temperatures or on a reaction between dibutylmagnesium and a dimethylsulfide borane complex [59], see reaction schemes (3) and (4). The initial product is complexed by the coordinating solvents, which can be removed in vacuum at temperatures below that of the irreversible phase transition from α- to β-Mg(BH₄)₂.



Ca(BH₄)₂ can be synthesized in a similar manner from triethylamine borane and CaH₂, or by a metathesis reaction in tetrahydrofuran [60].

Currently, wet chemistry synthesis methods are being investigated in more detail since it facilitates the synthesis of pure materials. At present, industrial scale-up facilities are better suited for wet chemistry approaches than for large scale mechano-chemical synthesis, thus research in the field of wet chemistry is highly desirable at least from a commercial point of view.

2.2 Mechano-chemistry Mechano-chemistry, e.g. ball milling, is a well established method for synthesis of new materials, homogenization, reduction of particle size and introduction of defects that facilitate hydrogen release and uptake [61]. The high reactivity observed for the mechanical milling of solids is not temperature driven since several studies reveal moderate temperatures (<60 °C)

during milling [62, 63]. The reaction is more likely driven by the ultra-high pressure induced by collisions between balls, vial and the powder, which may reach the GPa range and introduce deformations, e.g. by shear stress [64].

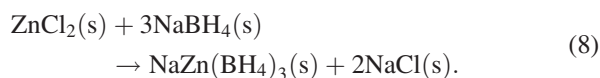
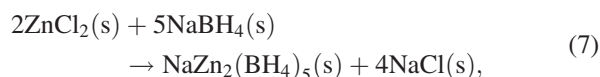
During ball milling a variety of reactions may occur and in some cases several competing reactions are observed simultaneously. Metathesis, or double substitution reaction, is a well known mechanism for chemical reactions during ball milling, here illustrated by the reaction between lithium borohydride, LiBH₄, and yttrium(III)chloride, YCl₃, which results in formation of Y(BH₄)₃ and LiCl according to reaction scheme (5) [65–69].



The system ZnCl₂–MBH₄, M = Li, Na and K, can be used to illustrate the complexity of mechano-chemistry. Ball milling a mixture of ZnCl₂–KBH₄ (1:1) leads to an addition reaction, see reaction scheme (6), and a phase pure product, of KZn(BH₄)Cl₂ [70].



The mechano-chemical synthesis of other new borohydrides in the system ZnCl₂–MBH₄ proceeds via more complex chemical reactions as for the synthesis of MZn₂(BH₄)₂, M = Li or Na and NaZn(BH₄)₃ described by reaction schemes (7) and (8) [48].



Reaction schemes (7) and (8) illustrate that small deviations in the composition of reactants may lead to significantly different reaction products.

These new compounds were prepared by ball milling in short intervals (2 min) separated by pauses (2 min) [48]. This procedure distributes the developed friction heat and keeps the temperature at room temperature suggesting that the synthesis is facilitated by the intrinsic high pressures developed during ball milling rather than elevated temperatures. In fact, this class of M-Zn-BH₄ compounds all decomposes irreversibly by heating at ~100 °C or by prolonged ball milling with release of diborane [48].

This observation also suggests that ball milling may lead to a chemical equilibrium state rather than just a statistical distribution of reactants [71–74]. However, reaction schemes (5), (7) and (8) also illustrate a general drawback of the mechano-chemical approach involving the metathesis reactions, namely that the product may be contaminated with an ionic compound formed as a side product.

Ionic-covalent type hydrides, i.e. complex hydrides, may also form solid solutions as well known for alloying of

metals, e.g. approximately 10% lithium chloride may dissolve in solid lithium borohydride by ball milling as described in reaction scheme (9) [75].



Furthermore, ball milling is useful for preparation of reactive hydride composites where intimate contact between particles of different hydrides is needed. The reduction of particle sizes by ball milling, i.e. increase of the surface area, also contributes to increase the reactivity of the materials.

In the view of potential future industrial production of hydrogen storage materials, an economical ton scale production is required. Commercial large scale mechanochemical techniques for grinding and activation of minerals is currently well established and can fairly easy be transferred to the synthesis of light metal hydrogen storage materials, although it may be relatively energy consuming [18, 61, 76].

2.3 Synthesis strategies for nanoconfined hydride systems

The most widely used technique for preparation of nano-sized metalhydride particles is ball milling [17]. In this top-down approach, described above, the size of the bulk material is reduced mechanically, in some cases to less than 100 nm. However, the samples are often contaminated with trace amounts of metals from vial and balls. Furthermore, sintering processes may occur such that the nano-sized particles grow into larger particles during hydrogen release and uptake cycles [77–80]. Nanoconfinement is a bottom-up approach that limits the particle size of the hydride to the pore size of the scaffold material, which allows direct production of smaller particles than obtainable mechanically by the ball milling technique. Furthermore, particle growth and agglomeration may be hindered by the compartmentalization of nanoparticles within the scaffold material, which also limits the mobility of the decomposition products and keeps them in intimate close contact.

Preparation of nanoconfined hydride systems is an important scheme to change the physical and chemical properties of the hydrides. The three most widely used methods to prepare nanoconfined hydride systems are briefly reviewed in the following section [30].

Melt infiltration can be used as an impregnation method when the melting point of the respective hydrides are lower than the decomposition temperature of the selected scaffold material. Although, the hydride itself may decompose upon melting, e.g. as observed for NaAlH_4 , which melts and starts to decompose to solid Na_3AlH_6 and Al at $T_{\text{mp}}(\text{NaAlH}_4) \sim 183^\circ\text{C}$ [81]. Elevated hydrogen pressures can suppress the decomposition and a typical procedure for melt infiltration of NaAlH_4 involves heating in the temperature range 180–190 °C in a reactor together with a porous material at a pressure of $p(\text{H}_2) = 160\text{--}190$ bar [34, 81–84]. Melt infiltration occurs due to a minimization of the total interfacial energy in the melt and support system.

The advantage is that solvents or precursor are not involved and post-treatment of the nanoconfined hydride composite is avoided. The disadvantage can be that many metals and their hydrides are very reactive in the molten state and the selection of a sufficiently inert scaffold material can be a challenge. Further information on melt infiltration can be found elsewhere [30, 85, 86].

Solvent mediated infiltration (also denoted wet infiltration) utilizes a solvent capable of dissolving and form a homogeneous solution of the compound to be infiltrated. The porous scaffold is submerged in the solution, which then infiltrates the pores. The hydride solidifies to form amorphous or crystalline solid nanoparticles in the pores upon removal of the solvent by evaporation. For example, NH_3BH_3 is readily soluble in methanol and such a solution (5.4 M) was infiltrated in an ordered mesoporous silica scaffold (SBA-15, $D_{\text{avg}} = 7.5$ nm). Excess methanol was subsequently removed by drying in vacuum and a loading of 50 wt% NH_3BH_3 in SBA-15 was obtained [87].

This method has the advantage that impregnation can be performed under more mild conditions as compared to the melt infiltration scheme. However, in some cases it can be a challenge to find a solvent that dissolves the material to be infiltrated without reacting with either the material or the porous scaffold. Furthermore, the solvent should be weakly coordinating to both the material and the scaffold, to allow removal of the solvent under moderate conditions. However, weakly coordinating solvents often dissolve a smaller amount of the compound to be infiltrated and therefore several cycles of impregnation may be needed [30].

Direct synthesis of nanoconfined metal hydrides. Nanoconfined magnesium hydride in resorcinol formaldehyde carbon aerogels, RF-CA, has been prepared using an organic precursor in solution; dibutylmagnesium, $\text{Mg}(\text{nBu})_2$, in heptane (1 M) [31, 88]. Dibutylmagnesium reacts with hydrogen at elevated temperatures and pressures, to form magnesium hydride nanoparticles and butane gas. This procedure was utilized for the direct synthesis of MgH_2 nanoparticles in monoliths of RF-CA carbon aerogels with average pore sizes of 22 and 7 nm [31]. The advantage of this approach is that surface excess white $\text{Mg}(\text{nBu})_2$ can be removed mechanically from the black RF-CA and that the amount of nanoconfined $\text{Mg}(\text{nBu})_2$ can be estimated from the weight gain of the aerogel monoliths [31].

3 Novel metal borohydrides The past few years have experienced a significant increase in both experimental and theoretical studies of new borohydrides and in particular on their structural and solid-state chemistry. The decomposition temperatures of single-cation borohydrides were recently found to be empirically related to the Pauling electronegativity of the cation [37]. The relation reveals that the higher the electronegativity of the metal cation the lower the decomposition temperature of the metal borohydride. Most known monometallic borohydrides of transition metals are too stable for practical applications [14]. The first bimetallic borohydride, $\text{LiK}(\text{BH}_4)_2$, recently obtained by

Nickels et al. [89] exhibits a decomposition temperature, which is nearly an average of those for the two alkali borohydrides. Although, for this particular example the decomposition temperature is also too high (the compound is based on two electropositive alkali metals), this suggests that preparation of bimetallic borohydrides based on an alkali or alkali earth and a metal with higher electronegativity, e.g. a transition metal, is a promising new route for tuning the thermodynamic properties of borohydride-based hydrogen storage materials [90].

As a result, a series of both novel mono- and bimetallic borohydrides mainly based on the fourth period transition metals have recently been prepared [48, 70, 91–96]. This new class of borohydride materials reveals a fascinating structural chemistry. The classical borohydrides based on the alkali metals exhibit predominantly ionic character in the metal-BH₄ coordination, mainly due to the low electronegativity of the metal and thus an almost complete charge transfer from the metal to the [BH₄][−] group. In contrast, directionality and some degree of covalent character in the metal-BH₄ bonding is observed in the novel metal borohydrides, where the more electronegative d-block metals show smaller charge transfer to the [BH₄][−] group, associated with destabilization of the latter unit.

There is no significant preference for the metals-BH₄ coordination mode in the ionic borohydrides, i.e. the [BH₄][−] units can be coordinated by metal atoms via the B-H corner, B-H₂ edge or B-H₃ face. This is clearly illustrated by the study of the pressure evolution of RbBH₄ at ambient temperature. The four RbBH₄ polymorphs show occurrence of three different Rb-BH₄ coordination modes: via a corner, edge or a face. Different arrangements of the tetrahedral [BH₄][−] group in the Rb environment define the crystal symmetries of the RbBH₄ polymorphs [97]. The resulting

close-packed structures correspond to the highly ionic bonding scheme in RbBH₄.

On the contrary, for the borohydrides, which presumably exhibit some degree of covalent metal-BH₄ bonding, stronger coordination preferences are observed, e.g. in framework structures where metal-BH₄ configurations are realized exclusively via BH₂ edges. This results in unexpected structural architectures and porosity, which is common for the coordination polymers involving organic ligands, such as MOFs [98]. However, this kind of frameworks were only recently observed in metal hydrides [48, 99]. These observations highlight the structure-forming character of the directional M-BH₄ interaction.

The new monometallic d-block borohydrides all form partly porous framework structures, whereas the bimetallic compounds containing both an alkali and a d-block metal tend to form structures built of discrete ions, usually a complex d-block metal borohydride anion counter-balanced by an alkali cation. The formation of discrete ions is most likely due to the relatively large difference in electronegativity between the two metals, which causes formation of partly covalent bonds between the more electronegative metal and the [BH₄][−] units. The formation of discrete metal borohydride anions or molecules might also be caused by highly polarising cations, e.g. Be²⁺ [100], Hf⁴⁺ [101] and Zr⁴⁺ [102]. These metals form molecular borohydrides, where some of the [BH₄][−] units are coordinated to one metal atom only.

In Table 1, the recently discovered metal borohydrides are grouped into framework structures and structures containing complex anions. It is interesting to note that only d-block metal borohydrides based on metals with d⁰, d⁵ or d¹⁰ electron configurations have been successfully obtained so far. This gives a hint that not only the electronegativity but

Table 1 Novel metal borohydrides divided into framework structures and structures containing complex anions. Their crystallographic space group symmetry, structural architecture and temperature of decomposition are listed.

compound	sp. gr.	structural architecture		<i>T</i> _{dec} (°C)	ref.	
framework structures						
Y(BH ₄) ₃	<i>Pa</i> -3	6-fold coordination of Y ³⁺ to [BH ₄] [−]		180 ^a	[67]	
	<i>Fm</i> -3 <i>c</i>	6-fold coordination of Y ³⁺ to [BH ₄] [−]		200	[65]	
NaY(BH ₄) ₂ Cl ₂	<i>P2</i> / <i>a</i>	6-fold coordination of Na ⁺ and Y ³⁺ to [BH ₄] [−] and Cl [−]		275	[103]	
Mn(BH ₄) ₂	<i>P3</i> ₁ 12	4-fold coordination of Mn ²⁺ to [BH ₄] [−]		177 ^b	[91]	
Mg _{1-x} Mn _x (BH ₄) ₂	<i>P3</i> ₁ 12	4-fold coordination of Mn ²⁺ or Mg ²⁺ to [BH ₄] [−]		— ^c	[92]	
compound	sp. gr.	cation	anion	structural architecture	<i>T</i> _{dec} (°C)	ref.
structures containing complex anions						
LiSc(BH ₄) ₄	<i>P</i> -42 <i>c</i>	Li ⁺	[Sc(BH ₄) ₄] [−]	8-fold coordination of [Sc(BH ₄) ₄] [−] to Li ⁺	211	[96]
NaSc(BH ₄) ₄	<i>Cmcm</i>	Na ⁺	[Sc(BH ₄) ₄] [−]	6-fold coordination of [Sc(BH ₄) ₄] [−] to Na ⁺	200	[93]
KSc(BH ₄) ₄	<i>Pnma</i>	K ⁺	[Sc(BH ₄) ₄] [−]	7-fold coordination of [Sc(BH ₄) ₄] [−] to K ⁺	210	[94]
LiZn ₂ (BH ₄) ₅	<i>Cmca</i>	Li ⁺	[Zn ₂ (BH ₄) ₅] [−]	doubly-interpenetrated framework	127	[48]
NaZn ₂ (BH ₄) ₅	<i>P2</i> ₁ / <i>c</i>	Na ⁺	[Zn ₂ (BH ₄) ₅] [−]	doubly-interpenetrated framework	95	[48]
NaZn(BH ₄) ₃	<i>P2</i> ₁ / <i>c</i>	Na ⁺	[Zn(BH ₄) ₃] [−]	8-fold coordination of [Zn(BH ₄) ₃] [−] to Na ⁺	103	[48]
KZn(BH ₄)Cl ₂	<i>P2</i> ₁ / <i>m</i>	K ⁺	[Zn(BH ₄)Cl ₂] [−]	7-fold coordination of [Zn(BH ₄)Cl ₂] [−] to K ⁺	120	[70]
Li ₄ Al ₃ (BH ₄) ₁₃	<i>P</i> -43 <i>n</i>	[(BH ₄)Li ₄] ³⁺	[Al(BH ₄) ₄] [−]	14-fold coordination of [Al(BH ₄) ₄] [−] to [(BH ₄)Li ₄] ³⁺	70	[104]

^aPhase transition to high temperature polymorph; ^bMelting with possible decomposition; ^cNot reported.

also the electron configurations of the metal may play a significant role in the stability of the borohydride.

3.1 Framework structures The first 3d-metal borohydride, $\text{Mn}(\text{BH}_4)_2$ has been prepared and characterized recently by Černý et al. [91]. The structure of $\text{Mn}(\text{BH}_4)_2$ shows a close similarity to that of $\alpha\text{-Mg}(\text{BH}_4)_2$ [99], both with respect to the local atom environment and in terms of the complex framework organization. Both independent manganese atoms are surrounded by four $[\text{BH}_4]^-$ units in a deformed tetrahedral coordination, while each $[\text{BH}_4]^-$ is nearly linearly coordinated by two Mn^{2+} cations via the opposite tetrahedral edges (Fig. 1). Moreover, the structure of $\text{Mn}(\text{BH}_4)_2$ is not densely packed and contains isolated voids with an estimated volume of 21 \AA^3 each. The voids occupy in total 6% of the space. Close similarity between $\text{Mn}(\text{BH}_4)_2$ and $\alpha\text{-Mg}(\text{BH}_4)_2$ is supported by the recent discovery of $\text{Mg}_x\text{Mn}_{1-x}(\text{BH}_4)_2$ solid solutions [92]. It is interesting to note that this compound retains the framework structure and no complex anions are formed. This is likely due to the small difference in electronegativity for the two metals ($\chi_p(\text{Mg}) = 1.31$, $\chi_p(\text{Mn}) = 1.55$) and their similar ionic radii.

Yttrium borohydride, $\text{Y}(\text{BH}_4)_3$ is another recently characterized monometallic borohydride. Two polymorphs, a low and a high temperature phase denoted α - and β - $\text{Y}(\text{BH}_4)_3$, respectively, were found [65, 66, 68, 69]. Transformation from α - to β - $\text{Y}(\text{BH}_4)_3$ is achieved by annealing in a narrow temperature interval of $177\text{--}202 \text{ }^\circ\text{C}$, as the decomposition occurs at higher temperatures. The high-temperature structure is stable on cooling. The cubic framework structures of the two polymorphs are closely related except for two major differences.

Firstly, in the low-temperature *Pa*-3 polymorph the octahedral environment for the Y atom is distorted [67],

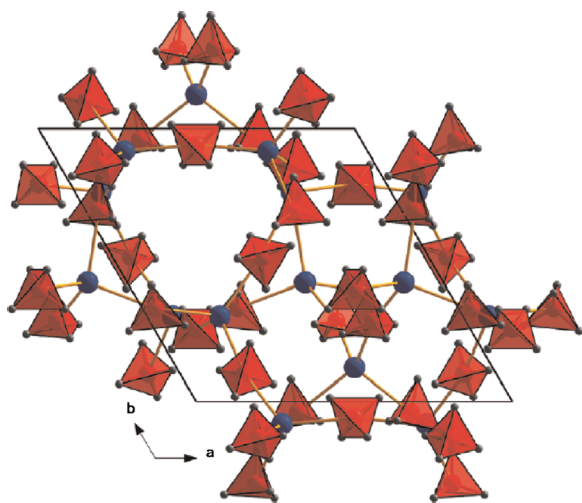


Figure 1 (online colour at: www.pss-a.com) The framework structure of $\text{Mn}(\text{BH}_4)_2$ (Mn: blue, BH_4 tetrahedra: red). The empty pore is situated approximately at $(0.304 \times 1/6)$ from which the shortest distance to the nearest atom (hydrogen) is 2.47 \AA [91].

while in the high-temperature *Fm*- $3c$ structure it is undistorted. Secondly, the high-temperature polymorph exhibits ordered arrangement of the $[\text{BH}_4]^-$ units, with half of them flipped in order to minimize H–H repulsion on the cost of a less densely packed structure [65]. This results in the high-temperature polymorph being 4.6% less dense than the low temperature one and it contains relatively large unoccupied voids of 39 \AA^3 , accounting for almost a quarter of the volume [66]. This underlines that $\beta\text{-Y}(\text{BH}_4)_3$, despite being isostructural to the ionic NaCl-type metal borohydride structures, exhibit some degree of directionality of the M– BH_4 bonding.

A mixed-cation mixed-anion yttrium borohydride, $\text{NaY}(\text{BH}_4)_2\text{Cl}_2$ has recently been characterized [103]. This compound is a 3D polymeric structure with no isolated complex anions, again likely due to the small difference in electronegativity between the metals ($\chi_p(\text{Na}) = 0.93$, $\chi_p(\text{Y}) = 1.22$). Introduction of a second anion, such as a halide or an amide ion [105], extends the structural diversity of metal borohydrides. Combining different ligands in modified metal borohydrides is one of the ways to adjust their stability with respect to hydrogen desorption.

3.2 Structures containing complex anions

Monometallic scandium borohydride has been reported several times as $\text{Sc}(\text{BH}_4)_3$, and a rhombohedral structural model has been predicted from theoretical calculations [37].

Nonetheless, no experimental evidence supporting the existence of $\text{Sc}(\text{BH}_4)_3$ is reported yet. However, three alkali metal–scandium borohydrides are known: $\text{LiSc}(\text{BH}_4)_4$, $\text{NaSc}(\text{BH}_4)_4$ and $\text{KSc}(\text{BH}_4)_4$ [93, 94, 96, 106]. The $\text{MSc}(\text{BH}_4)_4$ ($\text{M} = \text{Li, Na or K}$) compounds can be described as complexes containing discrete $[\text{Sc}(\text{BH}_4)_4]^-$ anions counter-balanced by the alkali metal cations. In all cases, the Sc atoms likely coordinate to the $[\text{BH}_4]^-$ groups via the faces, yielding a 12-fold coordination by H atoms. For $\text{NaSc}(\text{BH}_4)_4$ (Fig. 2) the Sc– BH_4 coordination forms nearly regular tetrahedra and resembles an almost ideal tetrahedral $[\text{Sc}(\text{BH}_4)_4]^-$ anion, as found by DFT optimization [96]. For both $\text{LiSc}(\text{BH}_4)_4$ and $\text{KSc}(\text{BH}_4)_4$ the experimentally observed anions are more distorted. The tetrahedral coordination of metal cations by four $[\text{BH}_4]^-$ units is also common for cations in many other metal borohydrides [38], e.g. Mg^{2+} in $\text{Mg}(\text{BH}_4)_2$ [99, 107], Li^+ in three of the four known phases of LiBH_4 [108–110], Hf^{4+} in $\text{Hf}(\text{BH}_4)_4$ [101] and Zr^{4+} in $\text{Zr}(\text{BH}_4)_4$ [102].

The $[\text{Sc}(\text{BH}_4)_4]^-$ anion in $\text{LiSc}(\text{BH}_4)_4$ is coordinated to eight Li^+ , which are disordered along the z axis of the tetragonal cell [96]. In the structure of $\text{NaSc}(\text{BH}_4)_4$ the $[\text{Sc}(\text{BH}_4)_4]^-$ anion is located inside slightly deformed trigonal prisms of Na^+ cations. The packing of Na^+ cations and $[\text{Sc}(\text{BH}_4)_4]^-$ anions is a distorted hexagonal NiAs structure type [93]. The structure of $\text{KSc}(\text{BH}_4)_4$ is of the BaSO_4 type where the $[\text{BH}_4]^-$ tetrahedra are on the positions of oxygen. Regarding the packing of K^+ cations and $[\text{Sc}(\text{BH}_4)_4]^-$ anions, the structure can be seen as a distorted variant of the orthorhombic Np metal structure type [94]. The

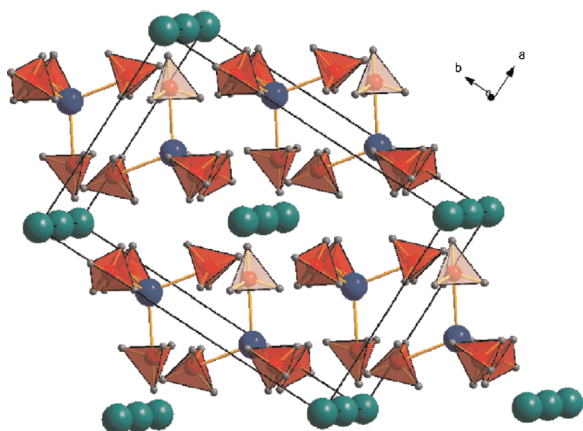


Figure 2 (online colour at: www.pss-a.com) Structure of $\text{NaSc}(\text{BH}_4)_4$ build from nearly regular tetrahedral $[\text{Sc}(\text{BH}_4)_4]^-$ anions coordinating to six Na^+ cations (Na: green, Sc: blue, $[\text{BH}_4]^-$ tetrahedra: red) [93].

structural organization in this series suggests a close packing of M^+ cations and $[\text{Sc}(\text{BH}_4)_4]^-$ anions, which underlines the discrete nature of the complex $[\text{Sc}(\text{BH}_4)_4]^-$ anions.

Zinc also forms a number of mixed-metal borohydrides with Li, Na and K. These are $\text{NaZn}(\text{BH}_4)_3$, $\text{LiZn}_2(\text{BH}_4)_5$, $\text{NaZn}_2(\text{BH}_4)_5$ [48] and $\text{KZn}(\text{BH}_4)\text{Cl}_2$ [70]. $\text{NaZn}(\text{BH}_4)_3$ shows a new type of structure, containing a 3D framework. Two independent synchrotron powder X-ray diffraction studies [48, 95] showed that Na^+ has a saddle-like coordination to the $[\text{BH}_4]^-$ groups, whereas Zn^{2+} has an intermediate coordination between a distorted tetrahedral and a flat-trigonal. DFT optimization of the experimental structures and IR spectra are consistent with the flat-trigonal coordination [95]. Hence, the compound may be rationalized as containing isolated $[\text{Zn}(\text{BH}_4)_3]^-$ anions counter-balanced by Na^+ cations.

The $\text{MZn}_2(\text{BH}_4)_5$ ($\text{M} = \text{Li}$ or Na) compounds represent a novel type of structures, which have no distinct analogues among other known inorganic compounds [48]. Remarkably, $\text{MZn}_2(\text{BH}_4)_5$ consists of two identical doubly-interpenetrated three-dimensional (3D) frameworks (Fig. 3) assembled by M^+ cations and $[\text{Zn}_2(\text{BH}_4)_5]^-$ anions. This type of structural topology signifies the directionality of the $\text{M}-\text{BH}_4$ interaction. Whereas such a structural architecture is common for the coordination of polymers involving organic ligands, characterization of $\text{MZn}_2(\text{BH}_4)_5$ revealed the first observation of such structures for metal hydrides.

Considering only the strongly associated Zn atoms and $[\text{BH}_4]^-$ units, $\text{MZn}_2(\text{BH}_4)_5$ compounds contain binuclear $[\text{Zn}_2(\text{BH}_4)_5]^-$ anions. The two independent Zn atoms in $[\text{Zn}_2(\text{BH}_4)_5]^-$ have a trigonal-planar coordination by three $[\text{BH}_4]^-$ groups, similar to the Be atoms in $\text{Be}(\text{BH}_4)_2$ [100]. The $[\text{BH}_4]^-$ groups are almost linearly coordinated by two metal atoms (the angles vary from 164.5° to 179.6°) via the two opposite edges, bridging either the two Zn atoms or coordinates to one Zn and one Li. Raman and IR studies of $\text{MZn}_2(\text{BH}_4)_5$ show that the $[\text{Zn}_2(\text{BH}_4)_5]^-$ anion contains

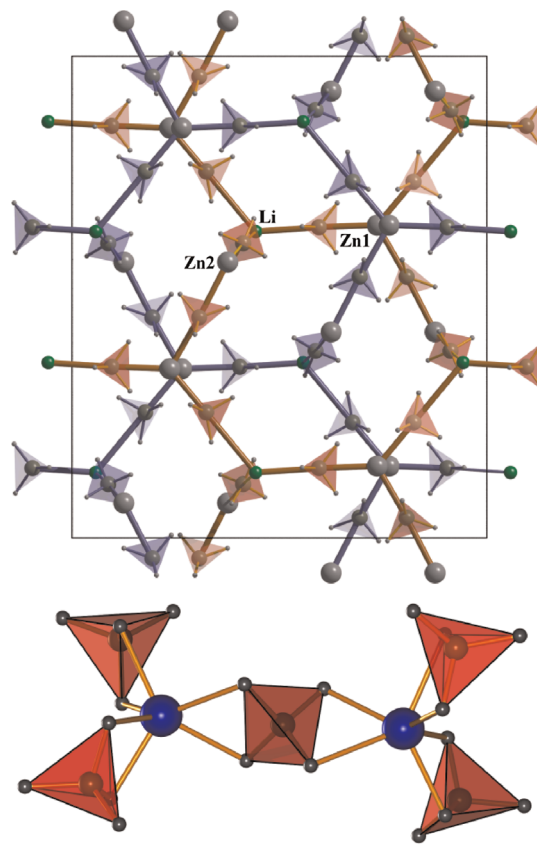


Figure 3 (online colour at: www.pss-a.com) Structure of $\text{LiZn}_2(\text{BH}_4)_5$ (a) build from doubly interpenetrated three-dimensional frameworks (highlighted in blue and red). Each framework consists of isolated dinuclear $[\text{Zn}_2(\text{BH}_4)_5]^-$ anions (b) counter balanced by Li^+ cations (Zn: blue, BH_4 tetrahedra: red) [48, 111].

both bridging and terminal $[\text{BH}_4]^-$ units, which underlines that the coordination to Zn is stronger than towards Li [95, 111].

Recently, the first heteroleptic complex anion has been structurally characterized. The complex anion $[\text{Zn}(\text{BH}_4)\text{Cl}_2]^-$ in $\text{KZn}(\text{BH}_4)\text{Cl}_2$ contains the Zn atom in a nearly flat trigonal coordination to one $[\text{BH}_4]^-$ and two Cl^- , which expands to tetrahedral coordination considering that zinc shares an edge with the $[\text{BH}_4]^-$ complex ion. The counter balancing K^+ cations has a 8-fold coordination towards five Cl^- and three $[\text{BH}_4]^-$ units acting as η^2 -ligands [70].

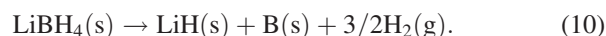
The most recent member of the growing family of borohydrides containing complex anions is $\text{Li}_4\text{Al}_3(\text{BH}_4)_{13}$ [104]. This compound is the first example of a bimetallic borohydride based on the s- and p-block metals. Its $P-43n$ structure was determined from synchrotron radiation powder X-ray diffraction (SR-PXD) data supported by DFT calculations [104]. Its unexpectedly complex composition can be rationalized on the basis of a complex cation $[(\text{BH}_4)\text{Li}_4]^{3+}$ and a complex anion $[\text{Al}(\text{BH}_4)_4]^-$. These two units are not isolated: Li-B distances within the $[(\text{BH}_4)\text{Li}_4]^{3+}$

complex and between the Li atom and $[\text{Al}(\text{BH}_4)_4]^-$ anion are similar, Also allowing the structure to be described as a 3D framework. Indeed, 12% porosity of the structure suggests that $\text{Li}_4\text{Al}_3(\text{BH}_4)_{13}$ is not closely packed, and therefore the directionality of metal-BH₄ interactions plays an important role. Rationalization of the bonding in terms of the complex anion and cation likely reflects these interactions and helps to explain the complex and unexpected stoichiometry.

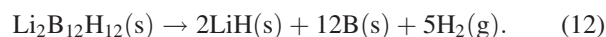
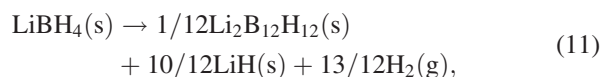
4 Decomposition mechanisms for borohydrides

A variety of borohydrides have been synthesized and structurally characterized during the past few years, however, their decomposition mechanism still remains poorly understood.

4.1 LiBH₄ The decomposition mechanism of lithium borohydride, LiBH₄, has received significant attention [112–115]. When LiBH₄ is heated, a polymorphic phase transition from orthorhombic to hexagonal structure takes place at 112 °C. LiBH₄ melts at approximately 275 °C, followed by decomposition, which mainly proceeds above 400 °C. The decomposition has been shown to follow reaction scheme (10), when LiBH₄ was kept at 600 °C for 5 min. under 1 bar of hydrogen pressure [116]. During decomposition at these conditions, 13.8 wt% H₂ is released from LiBH₄ since LiH is stable below 900 °C. The enthalpy change for the decomposition of LiBH₄, reaction scheme (10), is $\Delta H_d = 74 \text{ kJ/mol H}_2$ [36].



Furthermore, several unidentified compounds have been observed by *in situ* SR-PXD studies of LiBH₄ [112]. Computational studies suggest that monoclinic Li₂B₁₂H₁₂ is the most stable of several possible intermediate compounds ranging from LiB₃H₈ to Li₂B_nH_n ($n = 5\text{--}12$) [117]. Assuming that Li₂B₁₂H₁₂ is an intermediate compound during the decomposition a possible reaction is shown in reaction schemes (11) and (12):

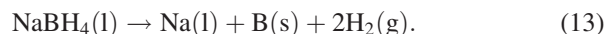


The enthalpy change for the decomposition of LiBH₄ according to reaction scheme (11), is 56 kJ/mol H₂ [118]. Raman spectroscopy investigations of LiBH₄ heated to 470 °C and $p(\text{H}_2) = 1$ bar reveal B-H bending and stretching modes around 600–1000 cm⁻¹ and 2500 cm⁻¹ and these values are comparable to the phonon density of states (PDOS) calculated for Li₂B₁₂H₁₂ [118]. The dehydrogenated LiBH₄, i.e., the mixture of LiH and B, can subsequently be rehydrogenated under conditions such as $p(\text{H}_2) \sim 70\text{--}350$ bar and $T \sim 600\text{--}650$ °C [11, 16, 18, 36, 116].

Lithium borohydride can be prepared by an addition reaction between lithiumhydride and diborane mediated by reactive ball milling ($p(\text{B}_2\text{H}_6) = 10$ bar for 30 h) [113]. LiBH₄ may also react with B₂H₆ at 200 °C for 40 h where diffraction from LiBH₄ was observed to be replaced by diffraction from Li₂B₁₂H₁₂ [119]. This may suggest that BH₃ or B₂H₆ may act as an intermediate during hydrogen release and uptake in borohydrides.

Release of diborane can be detected when lithium borohydride is decomposed in vacuum [120]. Diborane is known to decompose to hydrogen and higher boranes at $T > 50$ °C (depending on the diborane partial pressure). On the other hand, metal borides may form by reacting a metal and boron at 1000–2000 °C. This reaction may be facilitated by presence of a reducing agent, such as H₂ [121]. A hydrogen backpressure of $p(\text{H}_2) > 1$ bar, may therefore facilitate formation of a metal boride during decomposition of a metal borohydride at significantly lower temperatures as compared to the reaction between a metal and boron [122]. A backpressure of hydrogen is also desirable for practical applications. Formation of metal boride is essential in order to stabilize boron in the solid dehydrogenated state. Formation of diborane during decomposition leads to loss of boron and hydrogen storage capacity from the system. Furthermore, it was found that transition metal borides can be formed at *RT* by ball milling mixtures of LiBH₄, LiH and transition metal chlorides [123].

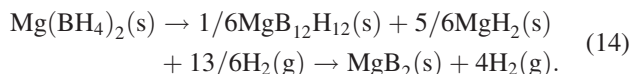
4.2 NaBH₄ Sodium borohydride, NaBH₄ ($\rho_m = 10.6$ wt%) decomposes at ~ 534 °C [124] to the parent elements (reaction scheme (13)), which are thermodynamically favoured due to the lower stability of NaH as compared to LiH formed in the decomposition of LiBH₄. Thermal analysis of NaBH₄ suggests that intermediate products may form during the decomposition [125].



4.3 KBH₄ The decomposition of KBH₄ ($\rho_m = 7.48$ wt%) follows a similar reaction as for NaBH₄, but occurs at slightly higher temperatures of ~ 585 °C [16, 126].

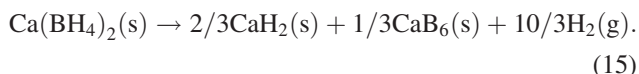
4.4 Mg(BH₄)₂ Magnesium borohydride, Mg(BH₄)₂, has a high gravimetric hydrogen content of 14.9 wt% H₂ and favourable thermodynamic properties, $\Delta H_d = 39.3$ kJ/mol H₂ ($p(\text{H}_2) = 1$ bar). A polymorphic phase transition from hexagonal to orthorhombic crystal structure, α - to β -Mg(BH₄)₂, takes place at 185 °C. Experimental data suggest that the dehydrogenation occurs in more than two steps at 290–350 °C forming H₂, Mg(B₁₂H₁₂), MgH₂ and finally MgB₂ [127–133]. The $[\text{B}_{12}\text{H}_{12}]^{2-}$ ion and MgB₂ was also detected by Raman spectroscopy when a dehydrogenated sample of Mg(BH₄)₂ was rehydrogenated at hydrogen pressure of 400 bar, 270 °C for 48 h in a Sieverts type apparatus. Reaction scheme (14) is therefore proposed as a

possible decomposition pathway [134, 135].



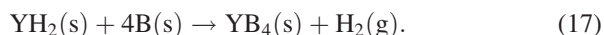
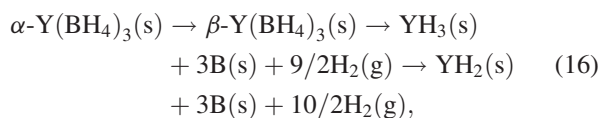
Direct hydrogenation of MgB_2 to $\text{Mg}(\text{BH}_4)_2$ is possible at 950 bar, 400 °C for 108 h. The presence of $\text{Mg}(\text{BH}_4)_2$ was confirmed with PXD analysis with a 75% yield and cyclic reversibility of 11 wt% H_2 was possible [127]. Amorphous magnesium borohydride may also be obtained by reactive ball milling of MgB_2 at room temperature and $p(\text{H}_2) = 100$ bar [136].

4.5 Ca(BH₄)₂ Calcium borohydride, $\text{Ca}(\text{BH}_4)_2$ ($\rho_m = 11.6$ wt%) undergoes a polymorphic phase transition, from α - to β - $\text{Ca}(\text{BH}_4)_2$, prior to decomposition at 527 °C where 9.4 wt% H_2 is released in accordance with reaction scheme (15) [137]. The expected decomposition reaction enthalpy change is 32 kJ/mol H_2 [138]. TG and DTA measurements indicate that intermediate compounds form during decomposition [137].



4.6 Transition metal borohydrides Borohydrides containing transition metals (see Section 3) generally decompose at lower temperatures than the alkali metal borohydrides. For $\text{LiSc}(\text{BH}_4)_4$ heated to approximately 500 °C in a Sieverts type apparatus the formation of the $[\text{B}_{12}\text{H}_{12}]^{2-}$ ion as an intermediate phase and ScB_2 as the end product were confirmed by ¹¹B MAS NMR [134].

Decomposition of $\text{Y}(\text{BH}_4)_3$ studied using *in situ* SR-PXD in the temperature range *RT* to 500 °C suggests the decomposition reaction as described by reaction schemes (16) and (17) [65, 66]. Rehydrogenating of $\text{Y}(\text{BH}_4)_3$ is possible at 260 °C and $p(\text{H}_2) = 35$ bar for 24 h [139].



4.7 Bialkali metal borohydrides A nearly linear relationship exists between the experimentally observed decomposition temperature and the electronegativity of the metal, which coordinates most strongly to the $[\text{BH}_4]^-$ groups (Table 1 and Fig. 4).

The decomposition temperature for the bialkali metal borohydride $\text{LiK}(\text{BH}_4)_2$ is approximately the average of the decomposition temperature for the mono alkali borohydrides, LiBH_4 and KBH_4 [35, 89]. For the only bimetallic

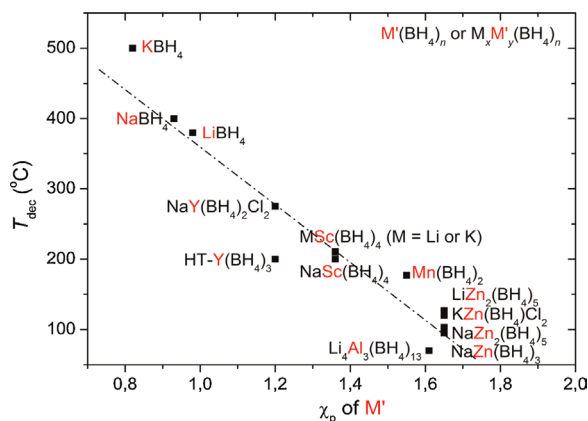


Figure 4 (online colour at: www.pss-a.com) Decomposition temperatures, T_{dec} for metal borohydrides plotted as a function of the electronegativity of the metal, M' . For the bimetallic borohydrides M' is the more electronegative of the two metals. Values for MBH_4 ($M = \text{Li}, \text{Na}$ and K) are from Ref. [35].

framework structure $\text{NaY}(\text{BH}_4)\text{Cl}_2$, the decomposition is observed at 75 °C higher than that of $\text{Y}(\text{BH}_4)_3$. This indicates that the presence of the alkali metal and possibly also the smaller chloride ion in the structure have a ‘stabilizing’ effect, i.e. T_{dec} comes closer to the average between those of NaBH_4 and $\text{Y}(\text{BH}_4)_3$. In contrast, borohydride structures containing complex anions, such as $[\text{Sc}(\text{BH}_4)_4]^-$ or $[\text{Zn}_2(\text{BH}_4)_5]^-$ in $\text{MSc}(\text{BH}_4)_4$ and $\text{MZn}_2(\text{BH}_4)_5$, show only minor variations in the decomposition temperature with changes in alkali metal. The strong correlation between the decomposition temperature and the electronegativity of the complex-forming metal indicates the key role of the complex anions in the structural stability of bimetallic borohydrides.

Furthermore, this short review clearly demonstrates that despite the fact that metal borohydrides have been investigated since the synthesis of $\text{Al}(\text{BH}_4)_3$ in 1939, there is still a lack of fundamental information on the decomposition reactions [49].

5 Anion substitution Anion substitution is a new and promising concept for tailoring the properties of known metal hydrides. Substitution of $[\text{BH}_4]^-$ or H^- by anions with the same charge and slightly different size may lead to formation of solid solutions. This type of substitution is well known for metals and ionic compounds and often occurs partially or in a limited range of the phase diagram. The relative size of the heavier halide anions and the $[\text{BH}_4]^-$ complex ion has been derived by comparison of the unit cell volumes for different inorganic salts to be $\text{I}^- > [\text{BH}_4]^- > \text{Br}^- > \text{Cl}^-$ [140]. The heavier halide ions and the $[\text{BH}_4]^-$ complex ion are of similar size and may substitute for each other.

On the other hand, the smaller halide, F^- , has similar size as the hydride ion, H^- , and these two compounds share many chemical properties, e.g. their ionic compounds are often found to be isostructural. This suggests that they may substitute for each other in both ionic and covalently bonded

compounds. Therefore, much research is devoted to study substitution of fluoride for hydride in, e.g. the $[\text{BH}_4]^-$ complex ion. This specific substitution, with the most electronegative element, is expected to change the bond strength of the remaining hydrogen atoms and thereby facilitate the release and possibly uptake of hydrogen [141].

5.1 Anion substitution using the heavier halides The heavier halides are found to readily substitute in some borohydrides and form solid-solution or stoichiometric compounds. Two stoichiometric compounds were discovered recently, $\text{KZn}(\text{BH}_4)\text{Cl}_2$ and $\text{NaY}(\text{BH}_4)\text{Cl}_2$, which were discussed in Sections 3.1 and 3.2 of this review. The metal borohydrides forming solid solutions upon halide substitution will be reviewed in the following.

5.1.1 LiBH_4 The first example of anion substitution in metal borohydride materials was reported in 2006 for a mixture of LiBH_4 – LiCl and observed in real time by *in situ* PXD [75, 142]. At a temperature of $\sim 120^\circ\text{C}$ the diffracted intensity of LiCl decreases simultaneously with an increase in the diffracted intensity of LiBH_4 (Fig. 5). This relationship between the intensities of LiCl and LiBH_4 suggests that solid LiCl dissolves in the structure of the solid hexagonal polymorph, h - LiBH_4 , which was unexpected due to the significant structural differences of the two compounds.

A more thorough investigation of the LiBH_4 – LiCl system utilizing Rietveld refinements of *in situ* SR-PXD data revealed a maximum chloride substitution of 42%, i.e. h - $\text{Li}(\text{BH}_4)_{0.58}\text{Cl}_{0.42}$ [41]. The substitution is clearly demonstrated in a plot of the unit cell volume per formula unit of $\text{Li}(\text{BH}_4)_{1-x}\text{Cl}_x$ versus temperature from $T = -73$ to 227°C (Fig. 6). The unit cell volume of orthorhombic o - LiBH_4 increases due to thermal expansion until the polymorphic phase transition o - to h - LiBH_4 occurs. The unit cell volume decreases for h - LiBH_4 despite the continuous heating due to dissolution of LiCl forming h - $\text{Li}(\text{BH}_4)_{1-x}\text{Cl}_x$, which is a fast

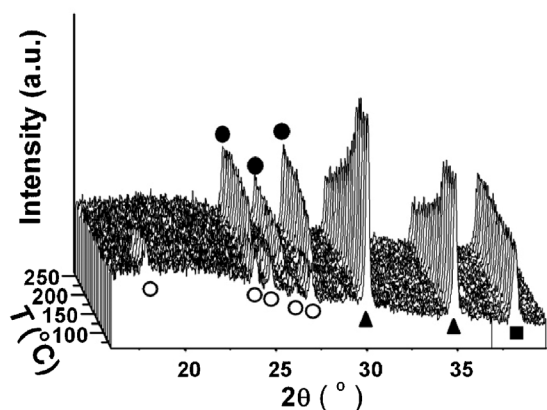


Figure 5 PXD patterns from LiBH_4 with 15 mol % LiCl heated from RT to 250°C showing a decrease in the diffracted intensity of LiCl at ca. 120°C , simultaneously with an increase in the diffracted intensity of LiBH_4 ($5^\circ\text{C}/\text{min}$, $\lambda = 1.54060 \text{ \AA}$). Symbols: \circ o - LiBH_4 , \bullet h - LiBH_4 , \blacktriangle LiCl , and \blacksquare Au (internal standard) [75].

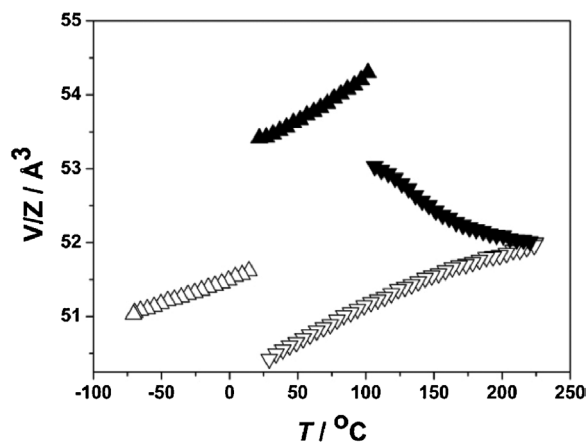


Figure 6 Unit cell volume per formula unit of the $\text{Li}(\text{BH}_4)_{1-x}\text{Cl}_x$ ($0.09 \leq x \leq 0.42$) structures for the first heating and cooling cycle. Symbols: \blacktriangle o - $\text{Li}(\text{BH}_4)_{1-x}\text{Cl}_x$ (heating), \blacktriangledown h - $\text{Li}(\text{BH}_4)_{1-x}\text{Cl}_x$ (heating), \triangle o - $\text{Li}(\text{BH}_4)_{1-x}\text{Cl}_x$ (cooling), \triangledown h - $\text{Li}(\text{BH}_4)_{1-x}\text{Cl}_x$ (cooling) [41].

reaction that occurs within minutes. The hexagonal solid solution, h - $\text{Li}(\text{BH}_4)_{0.58}\text{Cl}_{0.42}$, is stable upon cooling to RT. Slow segregation of LiCl from o - $\text{Li}(\text{BH}_4)_{1-x}\text{Cl}_x$ is observed to occur and a composition of h - $\text{Li}(\text{BH}_4)_{0.91}\text{Cl}_{0.09}$ is found after several months.

Substitution of bromide and iodide ions, in lithium borohydride occurs with similar trends as found for Cl^- substitution and provides a significant stabilization of the high temperature hexagonal polymorph [143, 144]. Furthermore, anion substitution in lithium borohydride significantly improves the lithium ion conductivity, which may be of importance for solid state lithium battery applications [145–148].

5.1.2 NaBH_4 The substitution of Cl^- with $[\text{BH}_4]^-$ in sodium borohydride has recently been investigated [149]. A large degree of substitution was discovered, i.e. up to 57% as revealed from Rietveld refinements of SR-PXD data. Furthermore, dissolution of small amounts of NaBH_4 in NaCl was also observed after prolonged heating at 300°C or facilitated by BM. However, with a dissolution rate, which is significantly slower as compared to the dissolution of NaCl in NaBH_4 .

5.1.3 KBH_4 The substitution of Cl^- for $[\text{BH}_4]^-$ in potassium borohydride was investigated for the system KBH_4 – ScCl_3 [94]. The anion substitution is observed during decomposition of $\text{KSc}(\text{BH}_4)_4$ where the two products formed, KBH_4 and K_3ScCl_6 , reacts to form a solid solution, $\text{K}(\text{BH}_4)_{1-x}\text{Cl}_x$, $0 < x < 0.97$, depending on the temperature [94].

5.1.4 $\text{Ca}(\text{BH}_4)_2$ Anion substitution in $\text{Ca}(\text{BH}_4)_2$ was first achieved by Lee et al. [40]. The degree of F^- and Cl^- substitution for the complex $[\text{BH}_4]^-$ -anion in $\text{Ca}(\text{BH}_4)_2$ was analysed and the dehydrogenation characteristics of the

substituted materials were investigated. The substitution was observed as a decreasing diffracted intensity from CaCl_2 and a reduction in the unit cell volume of $\text{Ca}(\text{BH}_4)_{2-x}\text{Cl}_x$ as compared to $\text{Ca}(\text{BH}_4)_2$, due to the smaller size of the chloride ion. The decomposition pathway of $\text{Ca}(\text{BH}_4)_{2-x}\text{Cl}_x$ differs from that of pure $\text{Ca}(\text{BH}_4)_2$, i.e. CaHCl and a new compound $\text{CaH}_{1.71}\text{Cl}_{0.29}$ forms.

Dissolution of I^- in $\text{Ca}(\text{BH}_4)_2$ is found to form three new crystalline solid solutions depending on the temperature [150]. Calcium borohydride readily dissolves in the trigonal calcium iodide structure during ball milling, forming a solid solution, *tri*- $\text{Ca}((\text{BH}_4)_{0.70}\text{I}_{0.36})_2$, with a CaI_2 -type structure and an anisotropically contracted trigonal unit cell, $a = 4.311(1)$ and $c = 6.867(2)$ Å for $x \sim 0.3$ ($T = 28^\circ\text{C}$), space group $P\bar{3}m1$. The trigonal *tri*- $\text{Ca}((\text{BH}_4)_{0.70}\text{I}_{0.30})_2$ transforms at $\sim 180^\circ\text{C}$ to an orthorhombic phase with similar composition, *ort*- $\text{Ca}((\text{BH}_4)_{0.64}\text{I}_{0.36})_2$, with a CaCl_2 -type structure (a distorted β - $\text{Ca}(\text{BH}_4)_2$ type structure), unit cell parameters $a = 7.271(2)$, $b = 7.042(1)$ and $c = 4.4601(7)$ Å ($T = 322^\circ\text{C}$) and space group $Pnmm$. Further heating of the CaCl_2 -type compound to $\sim 330^\circ\text{C}$ leads to a transition to a tetragonal phase with unit cell parameters $a = 4.1062(2)$ and $c = 24.822(2)$ Å ($T = 340^\circ\text{C}$, $x \sim 0.62$) and space group $I4mm$. This iodide-rich compound *tet*- $\text{Ca}((\text{BH}_4)_{0.38}\text{I}_{0.62})_2$, reveals a new structure type. The tetragonal phase finally decomposes to CaHI and CaB_6 at $T > 345^\circ\text{C}$. All three solid solutions found in the $\text{Ca}(\text{BH}_4)_2$ - CaI_2 system are stable at *RT*. The anion substitution ultimately changes the decomposition reaction pathway in which hydrogen is released from the tetragonal $\text{Ca}((\text{BH}_4)_{1-x}\text{I}_x)_2$ and via CaHI . Unfortunately the temperature of hydrogen release is still fairly high and similar to that for $\text{Ca}(\text{BH}_4)_2$ [150].

In contrast, CaF_2 did not dissolve in the structure of $\text{Ca}(\text{BH}_4)_2$ at the used physical conditions, however, during decomposition a solid solution of the CaH_2 - CaF_2 system was observed. Calculations suggests that $\text{Ca}(\text{BH}_{4-x}\text{F}_x)_2$ phases are thermodynamically unstable and decompose to $\text{Ca}(\text{BH}_4)_2$, CaF_2 , α -B and H_2 [40].

5.2 Fluoride substitution Substitution of the highly electronegative anion, F^- , for the hydride ion in the complex anions $[\text{BH}_4]^-$ or $[\text{AlH}_4]^-$ in metal hydrides was initiated by Kang et al. [151] already in 2007 during the study of the advantage of TiF_3 over TiCl_3 as an additive for the NaAlH_4 system. Experimental and theoretical studies show a destabilization of NaAlH_4 upon F^- substitution, giving an energy reduction on hydrogen release of 6.6 kJ/mol. A number of theoretical and experimental publications followed this study [152–154].

Theoretical calculations suggest that a similar effect is expected for the borohydride systems. Substitution of the hydride ion with the more electronegative fluoride ion, i.e. $\text{H}^- \rightarrow \text{F}^-$, is predicted to alter the hydrogen release and uptake properties for the LiBH_4 system significantly [155]. The F^- substitution in LiBH_4 is calculated to be an exothermic process. However, no experimental results on

the fluoride substitution in metal borohydrides have been reported yet.

The concept of anion substitution in borohydrides remains poorly explored, however, some trends in the structural chemistry are observed. For substitution of borohydrides with the heavier halides, the smaller anion tends to dissolve into the compound containing the larger anion, and the structure of the latter tends to be preserved in the obtained solid solution. This trend can be interpreted as an increase in the lattice energy due to the clearly observed decrease in the unit cell volume, i.e. a decrease in the average distance between the ions in the structure. Furthermore, anion substitution may ultimately change the decomposition reaction pathways with formation of decomposition products unique for these systems.

6 Reactive hydride composites The formation of alloys or intermetallic compounds according to reaction scheme (18) are well known approaches for the thermodynamic tuning of metal hydrides.



In the pioneering work by Libowitz et al. they observed much higher equilibrium desorption pressures of the ternary hydride ZrNiH_3 compared to the binary ZrH_2 at the same temperature, i.e. ZrNiH_3 appears to have a lower enthalpy of decomposition [156]. A huge amount of novel compounds with tailored thermodynamic properties have been discovered by this approach. A very prominent example for tuning of thermodynamic properties of light weight hydrides is the LiBH_4 -Al system forming LiH and AlB_2 in the desorbed state [157–162]. To overcome the drawback of the reduced gravimetric capacities of multinary systems, the reactive hydride composites (RHC) were recently developed [45, 46, 163–167]. In these, a chemical reaction between two or more hydrides during decomposition lowers the overall reaction enthalpy, while the gravimetric hydrogen storage capacity remains as high as the weighted hydrogen storage capacity of the individual hydrides. This concept is illustrated in Fig. 7, and the first prepared examples are the amide/imide systems shown in reaction schemes (19) and (20) [164, 165]:

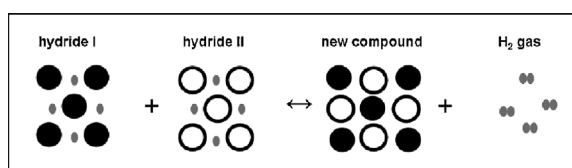
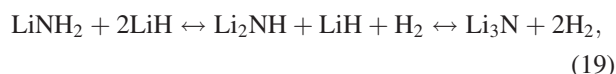
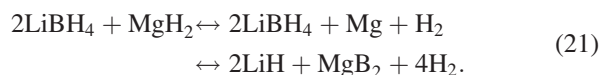


Figure 7 Schematic drawing of the concept of reactive hydride composites (RHC).

Other systems use the exothermic formation of a boride during the reaction between a light metal borohydride and another hydride. An example is the formation of MgB_2 from a borohydride and MgH_2 [163]. However, the combination of two borohydrides may also lead to an eutectic low melting mixture, which are the cases for the systems $\text{LiBH}_4\text{-Ca}(\text{BH}_4)_2$ and $\text{LiBH}_4\text{-Mg}(\text{BH}_4)_2$ [42, 168, 169].

Hydrogen release via reactions between a borohydride and a metal hydride forming a metal boride is observed for, e.g. $\text{LiBH}_4\text{-MgH}_2$, $\text{Ca}(\text{BH}_4)_2\text{-MgH}_2$, $\text{NaBH}_4\text{-MgH}_2$, $\text{LiBH}_4\text{-CaH}_2$, $\text{LiBH}_4\text{-CeH}_2$, $\text{LiBH}_4\text{-ScH}_2$ composites [42, 45, 163, 168, 170–177]. These systems reversibly absorb and release hydrogen. Theoretical calculations show promising reaction enthalpies for these composites, leading to suitable desorption pressures and temperatures for mobile applications combined with high gravimetric storage capacities. Furthermore, the reversibility of the borohydrides significantly benefits from the composite structure of the boride despite the reduced thermodynamic driving force [163]. As it requires extremely harsh conditions to produce LiBH_4 or $\text{Ca}(\text{BH}_4)_2$ from the elements [116, 138, 178], its formation through the gas phase is observed under moderate conditions starting from MgB_2 [163] or other boride precursors such as Li_7B_6 or CaB_6 [178, 179]. This is related to the higher reactivity of the metal borides in comparison to elemental boron.

Probably the most prominent and best studied example for RHC is the $2\text{LiBH}_4\text{-MgH}_2$ system reacting to form hydrogen, MgB_2 and LiH in the desorbed state, see reaction scheme (23) [18, 19, 43–45, 116, 122, 138, 163, 171, 172, 178–191]. This system shows a reversible hydrogen capacity of approximately 10.5 wt% and a theoretically assessed reaction enthalpy of 46 kJ/mol, leading to an estimated equilibrium temperature of 170 °C at 1 bar H_2 [45, 173]. The system has been studied extensively with respect to the reaction pathway, phase boundaries [44, 45, 174, 180, 181], the role and function of additives [37, 38, 50–52, 59] as well as the microstructure. However, the work is still ongoing, which illustrates the complexity of these composites. Especially important for the full reversibility and the suppression of B_2H_6 formation during the desorption reaction are the reaction conditions: a back pressure of 1–5 bar H_2 facilitates the formation of MgB_2 as it suppresses the individual decomposition of LiBH_4 [45, 122, 180]. The reaction according to reaction scheme (21) is illustrated by *in situ* SR-PXD measurements in Fig. 8 [44, 192].



The combined desorption reaction of LiBH_4 and the formation of MgB_2 under these conditions is shown elsewhere [180]. Possible reaction pathways and relations between the thermodynamic properties of the composite and the pure compounds as well as possible intermediate reactions are illustrated in the van't Hoff plot in Fig. 9, according to [180].

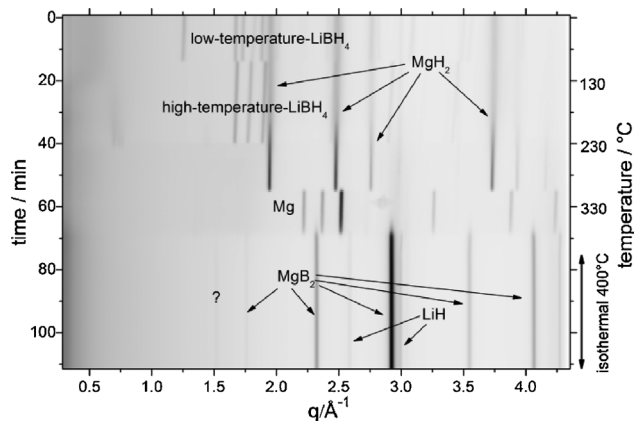


Figure 8 *In situ* SR-PXD of $\text{LiBH}_4\text{-MgH}_2$ composites with 5 mol% of a transition metal based additive. The $\text{LiBH}_4\text{-MgH}_2$ system was heated to 400 °C with 5 °C/min followed by isothermal conditions at $p(\text{H}_2) \sim 5$ bar [44, 192].

Since the formation of $\text{Li}_2\text{B}_{12}\text{H}_{12}$ was observed as an intermediate during the decomposition of LiBH_4 [114, 118, 134], its formation has also been discussed for the RHC system, which could be detrimental to the reversibility. Bösenberg et al. [180] related the possible presence of $\text{Li}_2\text{B}_{12}\text{H}_{12}$ to the reaction conditions depending on the thermodynamic properties.

A strong influence of transition metal based additives such as TiCl_3 , NiCl_2 or Ti-isopropoxide was observed. Detailed investigations of the X-ray absorption edge of the transition metals (XANES and EXAFS) showed the formation of nanoscale transition metal borides [183, 193–196]. Transition metal borides appear to support nucleation of MgB_2 and thus decrease the activation barrier and possibly improve the reaction kinetics and maybe leads to a refined microstructure [43, 194, 195].

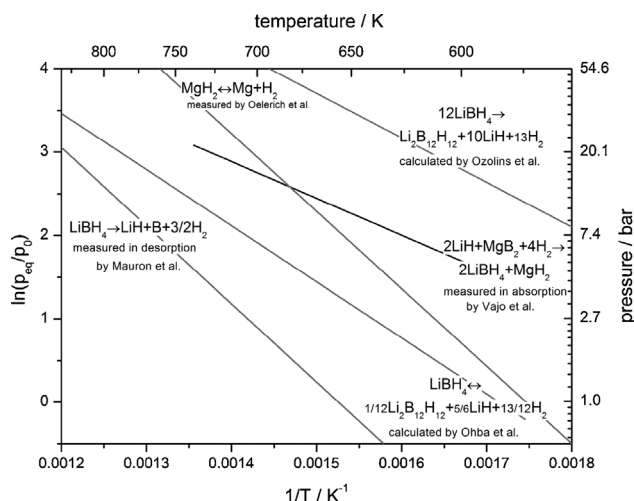


Figure 9 Van't Hoff diagram of the experimental and theoretically determined ΔH and ΔS for $\text{LiBH}_4\text{-MgH}_2$ composite as well as LiBH_4 and MgH_2 [18, 36, 45, 118, 182].

In comparison to $\text{LiBH}_4\text{-MgH}_2$, the $\text{Ca}(\text{BH}_4)_2\text{-MgH}_2$ system [170, 179, 197, 198] shows a much larger variety of reaction pathways and intermediate/final reaction steps, due to the possible formation of CaB_6 , $\text{Ca}_4\text{Mg}_3\text{H}_{14}$ and other Ca-B-H phases. Up to now, only partial reversibility of the composite according to the reaction $\text{CaH}_2 + \text{MgB}_2 \leftrightarrow \text{Ca}(\text{BH}_4)_2 + \text{MgH}_2$ has been obtained. It is interesting to note, that as in case of the $\text{LiBH}_4\text{-MgH}_2$ system, transition metal based additives seem to trigger the formation of MgB_2 in this system [199].

7 Nanoconfinement Nanoparticles may have significantly different properties as compared to bulk materials due to (i) increased surface area, (ii) nanoscale diffusion distances, (iii) increased number of atoms in the grain boundaries [200–203] and (iv) intimate contact between different reacting solids or a melt. These nanoscale properties often facilitate the release and uptake of hydrogen and thereby enhance the reaction kinetics. Furthermore, the thermodynamics may also be improved, and theoretical studies have predicted that increasing the surface area to bulk volume ratio destabilizes MgH_2 nanoparticles and thereby reduces the reaction enthalpy [17, 200, 204–206]. However, thermodynamic improvements are suggested to occur only for MgH_2 nanoparticles with a size less than 2–5 nm, while kinetic enhancement occurs also for larger nanoparticles below 30–50 nm [17, 77, 206, 207].

In the following, we review the use of nanoporous materials as scaffolds for preparation and confinement of nanosized metal hydrides and more details on this subject can be found elsewhere [30]. Nanoconfined chemistry is receiving increasing interest, e.g. for hydrogen storage and improvement of reaction kinetics and stability. In some cases improvement of thermodynamics of nanoconfined hydrides has also been reported [31, 29, 30, 81, 87, 208]. The development of fundamentally new nanomaterials is in general expected to have a major impact on the development of novel future sustainable energy technologies [30, 32].

7.1 MgH_2 Energy dispersive spectrometry (EDS) reveals that Mg/MgH_2 can be uniformly dispersed within resorcinol formaldehyde carbon aerogels (RF-CA) with pore sizes, $D_{\text{avg}} = 7$ and 22 nm, after preparation from dibutylmagnesium ($\text{Mg}(\text{nBu}_2)$) and are stable during subsequent cycling of hydrogen release and uptake at elevated temperatures [31]. PXD reveals Bragg peak broadening due to the small particle size of nanoconfined MgH_2 [88]. The highest gravimetric hydrogen storage capacity reported for nanoconfined MgH_2 is 1.40 wt% H_2 for 18.2 wt% MgH_2 loaded in RF-CA ($D_{\text{avg}} = 22$ nm) occupying 12 vol% of the available pore volume [31]. Higher gravimetric hydrogen capacities may be obtained by optimizing the infiltration procedures or by using several successive infiltrations. Hydrogen desorption kinetics was studied by means of temperature programmed desorption mass spectrometry, TPD-MS, (this method is also denoted thermal desorption spectroscopy, TDS), which demonstrates that smaller pores

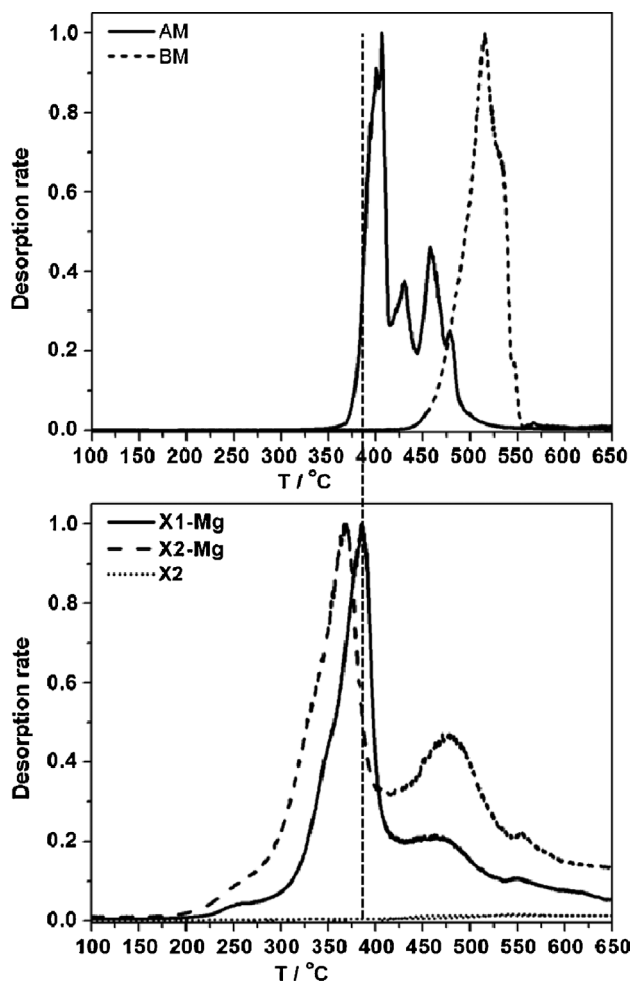


Figure 10 Normalized TPD-MS desorption profiles for samples of MgH_2 prepared from dibutylmagnesium without RF-CA (AM), bulk commercially available MgH_2 (BM), nanoconfined MgH_2 in RF-CA with 22 nm pores (X1-Mg), nanoconfined MgH_2 in RF-CA with 7 nm (X2-Mg) pores and pure RF-CA material (X2). The TPD-MS profile of sample X2 was normalized to the profile for sample X2-Mg. The samples were heated from RT to 700°C ($3.6^\circ\text{C}/\text{min}$) recording the mass spectroscopy, MS, signal ($m/e = 2$). The vertical line is drawn to guide the eye. The characteristic values for this kind of measurement is the onset temperature T_{onset} and also T_{max} where the desorption rate reaches its maximum value. Low T_{onset} and T_{max} values indicate faster kinetics [31].

mediate faster desorption rates, possibly due to a size reduction of the confined magnesium hydride, see Fig. 10 [31]. In this context, it should be noted that commercially available dibutylmagnesium in heptane solution contains up to 1 wt% triethylaluminum. Aluminum may influence the thermodynamic and kinetic properties of magnesium hydride by alloying [20, 31].

In general, there is a significant improvement of the hydrogen desorption kinetics for nanoconfined MgH_2 as compared to bulk samples as demonstrated by the Sieverts method [31, 88, 209]. The dehydrogenation rates at $T = 252^\circ\text{C}$ were determined to be 1.09 and $0.13 \text{ wt}\% \cdot \text{h}^{-1}$

for nanoconfined MgH_2 (13 nm RF-CA) and MgH_2 prepared from $\text{Mg}(\text{nBu}_2)$ and subsequent ball milling with graphite, respectively [88].

Initial hydrogen release rates at $T = 250^\circ\text{C}$ were found to be 25, 5.5, 2.2 and $0.12 \text{ wt}\% \cdot \text{h}^{-1}$ for MgH_2 melt infiltrated into Ni or Cu decorated RF-CA, non-modified RF-CA ($D_{\text{avg}} = 13 \text{ nm}$) and bulk MgH_2 ball milled with graphite, respectively [209]. It is noteworthy, that MgH_2 nanoconfined by melt infiltration of Mg desorbs hydrogen twice as fast as nanoconfined MgH_2 prepared using an organic precursor [88, 209]. The most significant improvements of hydrogen release kinetics for MgH_2 were obtained by the combined use of nanoconfinement and the catalytic metal additives such as, e.g. Ni and Cu [209, 210]. Furthermore, metallic surface decoration of carbonaceous porous scaffolds is found to facilitate the melt infiltration of magnesium [85, 209, 211]. The nanoconfinement of MgH_2 and the use of metallic nanoparticles as catalysts may hold the key to a significant improvement of the hydrogen release and uptake kinetics, but the scheme needs to be further developed in order to exceed hydrogen release rates of $25\text{--}50 \text{ wt}\% \text{ h}^{-1}$ as determined for ball milled samples of MgH_2 and Nb_2O_5 [88, 209, 210, 212].

7.2 $2\text{LiBH}_4\text{-MgH}_2$ Recently, $2\text{LiBH}_4\text{-MgH}_2$ reactive hydride composites (RHC) were infiltrated in a nanoporous RF-CA scaffold ($D_{\text{avg}} \sim 21 \text{ nm}$) in an attempt to combine the beneficial effect from nanoconfinement and reactive hydride composites. The nanoconfined hydrides reacted following the reaction shown in scheme (21) as observed for the bulk system. However, in these studies an Al impurity (present in the used dibutylmagnesium solution) was present and the formation of $\text{Mg}_x\text{Al}_{1-x}\text{B}_2$ phases was observed which to some extent hampers the conclusions [29]. The hydrogen desorption mechanism was also investigated using simultaneous differential scanning calorimetry, thermogravimetric analysis and mass spectrometry (DSC-TGA-MS) as depicted in Fig. 11.

The DSC analysis reveals four distinct endothermic desorption peaks denoted A, B, C and D for both samples, but observed at significantly different temperatures. Peaks A and B are observed at 113 and 267°C and at 117 and 290°C for the nanoconfined and the bulk hydride composite, respectively (peak temperature values are given). These events, A and B, are assigned to the transformation from orthorhombic to hexagonal structure and the melting of LiBH_4 , respectively. The thermal events C and D are observed at 332°C and $\sim 351^\circ\text{C}$ and at 364°C and $\sim 462^\circ\text{C}$ for the nanoconfined and the bulk composite hydrides, respectively. Events C and D reveal a mass loss from the hydride composites in the form of hydrogen gas and are assigned to the dehydrogenation of MgH_2 and LiBH_4 , respectively.

The results in Fig. 11 clearly demonstrate that nanoconfinement of $2\text{LiBH}_4\text{-MgH}_2$ significantly improves the hydrogen desorption kinetics for both hydrides. It is also clear that nanoconfinement mediates a larger reduction in the decomposition temperature for LiBH_4 as compared to MgH_2

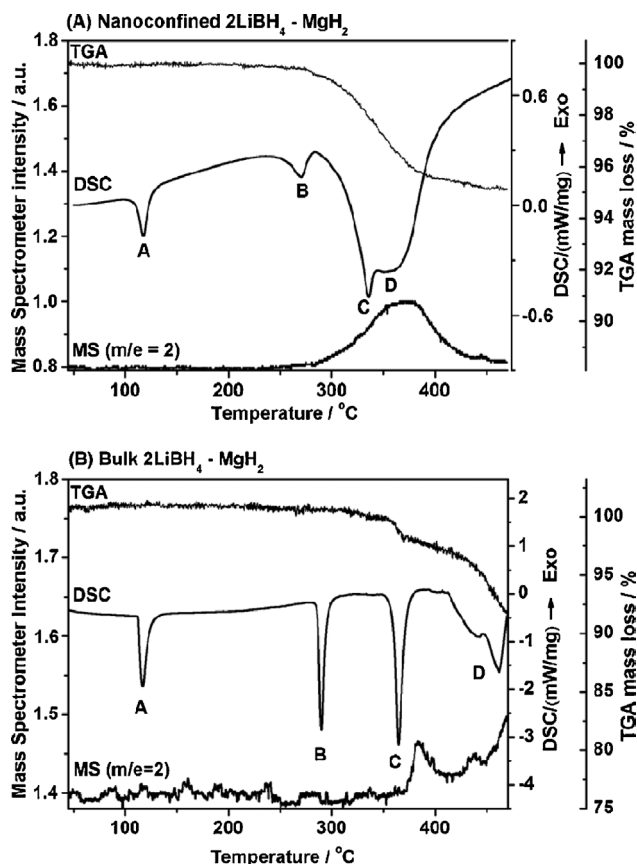
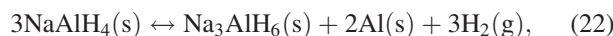
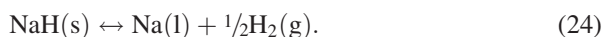


Figure 11 Simultaneous differential scanning calorimetry, thermogravimetric analysis and mass spectrometry showing the hydrogen release reactions from nanoconfined and bulk $2\text{LiBH}_4\text{-MgH}_2$. Two cycles of hydrogen release and uptake in magnesium synthesized from $\text{Mg}(\text{nBu}_2)$ was conducted prior to melt infiltration of LiBH_4 in both samples, (A) nanoconfined sample of $2\text{LiBH}_4\text{-MgH}_2$ in RF-CA ($D_{\text{avg}} = 21 \text{ nm}$) and (B) bulk sample of $2\text{LiBH}_4\text{-MgH}_2$. The samples were heated from RT to 470°C (heating rate $5^\circ\text{C}/\text{min}$ in an argon flow of $50 \text{ mL}/\text{min}$) [29].

[31, 29]. It has been demonstrated that fullerene, C_{60} , has a good catalytic effect on the hydrogen release and uptake of LiBH_4 [213]. The RF-CA scaffold may have a similar catalytic effect on LiBH_4 in addition to the nanoconfinement. Apparently, nanoconfinement mediates a change in the decomposition pathway of LiBH_4 thereby enhancing the hydrogen release kinetics. The decomposition pathway for MgH_2 remains less affected and magnesium is an intermediate prior to the formation of MgB_2 .

7.3 NaAlH_4 Sodium tetrahydridoalane was the first complex metal hydride to be considered for hydrogen storage. NaAlH_4 has a gravimetric hydrogen content of 7.4 wt% H_2 and is known to release hydrogen in three steps, see reaction schemes (22)–(24):





The enthalpies for hydrogen release in the three reactions are $\Delta H_{\text{d}} = 37$, 47 and 56 kJ/mol H_2 , respectively. Equilibrium temperatures, T_{eq} , can be calculated for reactions (22) and (23) using the Van't Hoff equation, $p(\text{H}_2) = 1$ bar and the ΔH_{d} values to be $T_{\text{eq}} = 30$ and 100 °C, respectively. However, due to kinetic limitations the hydrogen decomposition only take place at higher temperatures of $T > 180$ and 240 °C and the rehydrogenation also suffers from slow kinetics [34, 81]. However, it has been reported that improved hydrogen uptake and release kinetics can be obtained by addition of Ti, Sc or Ce based catalysts [33, 34, 214–216].

Nanoconfinement of NaAlH_4 leads to enhanced hydrogen release and uptake kinetics at more mild conditions e.g. melt infiltrated NaAlH_4 in RF-CA ($D_{\text{avg}} = 13$ nm) releases hydrogen at $T_{\text{onset}} \sim 140$ °C and absorb 85% of the initial H_2 content at 160 °C, $p(\text{H}_2) = 100$ bar H_2 within 7 h [82]. Ball milled NaAlH_4 release hydrogen at $T \sim 183$ °C. Carbon additives such as fullerene and carbon nanotubes are known to facilitate hydrogen release and uptake in NaAlH_4 and therefore nanoporous carbon materials may simultaneously act as a catalyst and as a scaffold for nanoconfinement [45, 163]. Furthermore, nanoconfinement in very small nanopores (3 nm) mediates a change in thermodynamic properties with the stabilization of NaAlH_4 as hydrogenated state and $\text{NaH} + \text{Al}$ as dehydrogenated state and thereby a suppression of the intermediate Na_3AlH_6 . For example, pressure composition isotherms (PCI) of bulk NaAlH_4 (catalysed with 4 mol% TiCl_3) show two distinct plateaus representing the equilibriums of the two reaction steps (22) and (23), respectively. However, the same analysis of nanoconfined NaAlH_4 in activated carbon (AC) fibres ($D_{\text{avg}} = 0.5$ to 4 nm) reveals a different PCI curve exhibiting a broad distribution of thermodynamic properties and NaAlH_4 seems to be stabilized due to nanoconfinement [82]. Moreover, ^{27}Al solid state NMR studies of nanoconfined NaAlH_4 in nanoporous carbon ($D_{\text{avg}} = 2$ –3 nm) indicated no presence of Na_3AlH_6 in partially dehydrogenated samples or samples that had been hydrogenated under conditions in which Na_3AlH_6 is the thermodynamically stable phase for the bulk system. This indicates that nanoconfinement of NaAlH_4 in very small nanopores (~ 3 nm) mediates a change in the kinetic or thermodynamic properties with the stabilization of NaAlH_4 as hydrogenated state and $\text{NaH} + \text{Al}$ as dehydrogenated state and thereby a suppression of the intermediate Na_3AlH_6 [32, 81, 82]. These observations correspond with theoretical studies [217]. However, experimentally determined thermodynamic improvements may also be due to systematic errors such as release of gasses from the scaffold material, reactions with the scaffold or the influence of impurities. Although, nanoconfinement of NaAlH_4 leads to significantly improved

hydrogen storage properties, titanium catalysed NaAlH_4 remains a superior system [84]. However, a new nanoconfined NaAlH_4 – TiCl_3 material was recently investigated and the hydrogen desorption kinetics was significantly improved as compared to bulk ball milled samples of NaAlH_4 – TiCl_3 indicating favorable synergetic effects between nanoconfinement and the addition of a catalyst [218].

7.3.1 NH_3BH_3 Ammonia borane has a gravimetric hydrogen content of 19.6 wt% H_2 . Thermal decomposition of ammonia borane takes place upon melting ($T_{\text{m}}(\text{NH}_3\text{BH}_3) = 114$ °C) with the release of 6.5 wt% H_2 and formation of poly(aminoboranes), $(\text{NH}_2\text{BH}_2)_n$. At temperatures above 150 °C, a polyiminoborane type material $(\text{NHBH})_n$ forms along with a second equivalent of hydrogen [87, 219]. The use of ammonia borane for practical applications is hampered by relatively slow kinetics, lack of reversibility and formation of undesired borazine gas, which is harmful to PEM fuel cells [87, 220]. Improved hydrogen desorption kinetics of NH_3BH_3 infiltrated in ordered mesoporous silica (SBA-15 and MCM-41) and nanoporous carbon scaffolds (OMC and RF-CC) as compared to bulk NH_3BH_3 , has been reported [87, 212, 220, 221]. Apparent activation energies, E_{A} , for hydrogen release from bulk and nanoconfined NH_3BH_3 were found to be ~ 184 and 67 kJ/mol, respectively [87]. As opposed to most metal hydrides the enthalpy of decomposition for NH_3BH_3 is exothermic, $\Delta H_{\text{dec}} = -19.6$ kJ/mol [213]. The value for NH_3BH_3 infiltrated in SBA-15 is $\Delta H_{\text{dec}} = -1$ kJ/mol, and it is suggested that this significant change in the thermodynamics is due to the formation of different borane based decomposition products as indicated by ^{11}B NMR studies [87]. These results indicate that the decomposition reaction mechanism is modified significantly by the nanoconfinement or that there is a reaction with the scaffold [220]. For all the systems discussed above, the release of borazine during the decomposition of NH_3BH_3 was suppressed by nanoconfinement [87, 220, 221]. Furthermore, the release of NH_3 from NH_3BH_3 can be suppressed by nanoconfinement in OMC combined with lithium cation doping, which also appear to improve the hydrogen desorption kinetics further [220].

8 Conclusion A major challenge in the 21st century is the transition towards a sustainable, environmentally friendly and reliable energy system capable of meeting the worlds increasing energy demands. In an energy system dominantly based on a diverse mix of renewable energy sources it is mandatory to have a storage system to balance the daily and seasonal fluctuations in energy production and consumption. In this context hydrogen is suggested as a possible future energy carrier.

This review highlights the recent progress within the field of hydrogen storage with focus mainly on new synthesis methods and physical, chemical and structural properties of boron based materials. New approaches for improving kinetic and thermodynamic properties are reviewed: (i) anion substitution, (ii) reactive hydride composites and

(iii) nanoconfinement of hydrides and chemical reactions. Anion substitution may lead to new solid solutions. Reactions between different hydrides are an efficient way to tailor the reaction thermodynamics. Nanoconfinement is an emerging powerful tool for tailoring kinetic and thermodynamic properties of chemical reactions for a variety of purposes. Furthermore, the novel light metal borohydrides, reveal a fascinating structural chemistry and have the potential for storing large amounts of hydrogen. Design of novel borohydrides by selection of coordinating metals may tailor the hydrogen release temperatures. We anticipate that utilization of the above mentioned schemes either alone or in new combinations have the potential to further expand the variety of materials and composites that are presently considered for hydrogen storage purposes. The present review may provide new inspiration for the possible discovery of new means of solid state hydrogen storage.

Acknowledgements The European Commission (contract NMP-2008-261/FLYHY) and the Danish Research Council for Natural Sciences (Danscatt) is thanked for financial support. The work was also supported by the Danish National Research Foundation (Centre for Materials Crystallography), the Danish Strategic Research Council (Centre for Energy Materials) and the Carlsberg Foundation.

References

- [1] International Energy Outlook, U.S. Energy Information Administration Office of Integrated Analysis and Forecasting (U.S. Department of Energy, Washington, DC 20585, 2010).
- [2] J. R. Petit, J. Jouzel, D. Raynaud, N. I. Barkov, J. Barnola, I. Basile, M. Bender, J. Chappellaz, M. Davis, G. Delaygue, M. Delmotte, V. M. Kotlyakov, M. Legrand, V. Y. Lipenkov, C. Lorius, L. Pépin, C. Ritz, E. Saltzman, and M. Stievenard, *Nature* **399**, 429–436 (1999).
- [3] *Nature Mater.* **8**, 81 (2009).
- [4] IPCC, Climate Change 2007, Synthesis Report (http://www.ipcc.ch/Pdf/Assessment-Report/Ar4/Syr/Ar4_syr.pdf, 2007).
- [5] P. D. Jones, T. J. Osborn, and K. R. Briffa, *Science* **292**, 662–667 (2001).
- [6] K. Caldeira, A. K. Jain, and M. I. Hoffert, *Science* **299**, 2052–2054 (2003).
- [7] D. J. C. MacKay, *Sustainable Energy – Without the Hot Air* (UIT, Cambridge, 2009).
- [8] N. Armaroli and V. Balzani, *Angew. Chem. Int. Ed.* **46**, 52–66 (2007).
- [9] A. Züttel, *Naturwissenschaften* **91**, 157–172 (2004).
- [10] A. Züttel, A. Borgschulte, and L. Schlapbach, *Hydrogen as a Future Energy Carrier* (Wiley-VCH, Weinheim, 2008).
- [11] L. Schlapbach and A. Züttel, *Nature* **414**, 353–358 (2001).
- [12] J. A. Ritter, A. D. Ebner, J. Wang, and R. Zidan, *Mater. Today* **6**, 18–23 (2003).
- [13] M. Felderhoff, C. Weidenthaler, R. Helmolt, and U. Eberle, *Phys. Chem. Chem. Phys.* **9**, 2643–2653 (2007).
- [14] W. Grochala and P. P. Edwards, *Chem. Rev.* **104**, 1283–1316 (2004).
- [15] M. Hirscher, *Handbook of Hydrogen Storage* (Wiley-VCH, Weinheim, 2010).
- [16] S. I. Orimo, Y. Nakamori, J. R. Eliseo, A. Züttel, and C. M. Jensen, *Chem. Rev.* **107**, 4111–4132 (2007).
- [17] M. Paskevicius, D. A. Sheppard, and C. E. Buckley, *J. Am. Chem. Soc.* **132**, 5077–5083 (2010).
- [18] M. Dornheim, N. Eigen, G. Barkhordarian, T. Klassen, and R. Bormann, *Adv. Eng. Mater.* **8**, 377–385 (2006).
- [19] M. Dornheim, S. Doppiu, G. Barkhordarian, U. Bösenberg, T. Klassen, O. Gutfleisch, and R. Bormann, *Scr. Mater.* **56**, 841–846 (2007).
- [20] A. Andreasen, M. B. Sørensen, R. Burkarl, B. Møller, A. M. Molenbroek, A. S. Pedersen, J. W. Andreasen, M. M. Nielsen, and T. R. Jensen, *J. Alloys Compd.* **404**, 323–326 (2005).
- [21] A. Andreasen, M. B. Sørensen, R. Burkarl, B. Møller, A. M. Molenbroek, A. S. Pedersen, T. Vegge, and T. R. Jensen, *Appl. Phys. A* **82**, 515–521 (2006).
- [22] T. R. Jensen, A. Andreasen, T. Vegge, J. W. Andreasen, K. Stahl, A. S. Pedersen, M. M. Nielsen, A. M. Molenbroek, and F. Besenbacher, *Int. J. Hydrogen Energy* **31**, 2052–2062 (2006).
- [23] J. Lu, Y. J. Choi, Z. Z. Fang, H. Y. Sohn, and E. Rönnebro, *J. Am. Chem. Soc.* **131**, 15843–15852 (2009).
- [24] D. Zander, L. Lyubenova, U. Koster, M. Dornheim, F. Aguey-Zinsou, and T. Klassen, *J. Alloys Compd.* **413**, 298–301 (2006).
- [25] D. Zander, L. Lyubenova, U. Koster, T. Klassen, and M. Dornheim, *J. Alloys Compd.* **434**, 753–755 (2007).
- [26] M. Polanski, T. Plocinski, I. Kunce, and J. Bystrzycki, *Int. J. Hydrogen Energy* **35**, 1257–1266 (2010).
- [27] M. Polanski, T. K. Nielsen, Y. Cerenius, J. Bystrzycki, and T. R. Jensen, *Int. J. Hydrogen Energy* **35**, 3578–3582 (2010).
- [28] R. L. Corey, T. M. Ivancic, D. T. Shane, E. A. Carl, R. C. Bowman, J. M. B. von Colbe, M. Dornheim, R. Bormann, J. Huot, R. Zidan, A. C. Stowe, and M. S. Conradi, *J. Phys. Chem. C* **112**, 19784–19790 (2008).
- [29] T. K. Nielsen, U. Bösenberg, R. Goslawit, M. Dornheim, Y. Cerenius, F. Besenbacher, and T. R. Jensen, *ACS Nano* **4**, 3903–3908 (2010).
- [30] T. K. Nielsen, F. Besenbacher, and T. R. Jensen, *Nanoscale* **3**, 2086 (2011).
- [31] T. K. Nielsen, K. Manickam, M. Hirscher, F. Besenbacher, and T. R. Jensen, *ACS Nano* **3**, 3521–3528 (2009).
- [32] P. E. de Jongh and P. Adelhelm, *ChemSusChem* **3**, 1332–1348 (2010).
- [33] B. Bogdanović and M. Schwickardi, *J. Alloys Compd.* **253**, 1–9 (1997).
- [34] B. Bogdanović, R. A. Brand, A. Marjanović, M. Schwickardi, and J. Tölle, *J. Alloys Compd.* **302**, 36–58 (2000).
- [35] A. Züttel, S. Rentsch, P. Fischer, P. Wenger, P. Sudan, P. Mauron, and C. Emmenegger, *J. Alloys Compd.* **356/357**, 515–520 (2003).
- [36] P. Mauron, F. Buchter, O. Friedrichs, A. Remhof, M. Biemann, C. N. Zwicky, and A. Züttel, *J. Phys. Chem. B* **112**, 906–910 (2008).
- [37] Y. Nakamori, K. Miwa, A. Ninomiya, H. Li, N. Ohba, S. Towata, A. Züttel, and S. I. Orimo, *Phys. Rev. B* **74**, 45126 (2006).

- [38] Y. Filinchuk, D. Chernyshov, and V. Dmitriev, *Z. Kristallogr.* **223**, 649–659 (2008).
- [39] D. B. Ravnsbæk, Y. Filinchuk, R. Černý, and T. R. Jensen, *Z. Kristallogr.* **225**, 557–569 (2010).
- [40] J. Y. Lee, Y. Lee, J. Suh, J. Shim, and Y. W. Cho, *J. Alloys Compd.* **506**, 721–727 (2010).
- [41] L. M. Arnbjerg, D. B. Ravnsbæk, Y. Filinchuk, R. T. Vang, Y. Cerenius, F. Besenbacher, J. E. Jørgensen, H. J. Jakobsen, and T. R. Jensen, *Chem. Mater.* **21**, 5772–5782 (2009).
- [42] J. Y. Lee, D. Ravnsbæk, Y. Lee, Y. Kim, Y. Cerenius, J. Shim, T. R. Jensen, N. H. Hur, and Y. W. Cho, *J. Phys. Chem. C* **113**, 15080–15086 (2009).
- [43] U. Bösenberg, J. W. Kim, D. Goslar, N. Eigen, T. R. Jensen, J. M. von Colbe, Y. Zhou, M. Dahms, D. H. Kim, R. Günther, Y. W. Cho, K. H. Oh, T. Klassen, R. Bormann, and M. Dornheim, *Acta Mater.* **58**, 3381–3389 (2010).
- [44] U. Bösenberg, S. Doppiu, L. Mosegaard, G. Barkhordarian, N. Eigen, A. Borgschulte, T. R. Jensen, Y. Cerenius, O. Gutfleisch, T. Klassen, M. Dornheim, and R. Bormann, *Acta Mater.* **55**, 3951–3958 (2007).
- [45] J. J. Vajo, S. L. Skeith, and F. Mertens, *J. Phys. Chem. B* **109**, 3719–3722 (2005).
- [46] Y. W. Cho, J. Shim, and B. Lee, *Calphad* **30**, 65–69 (2006).
- [47] H. Hagemann and R. Černý, *Dalton Trans.* **39**, 6006–6012 (2010).
- [48] D. B. Ravnsbæk, Y. Filinchuk, Y. Cerenius, H. J. Jakobsen, F. Besenbacher, J. Skibsted, and T. R. Jensen, *Angew. Chem. Int. Ed.* **48**, 6659–6663 (2009).
- [49] H. I. Schlesinger, R. T. Sanderson, and A. B. Burg, *J. Am. Chem. Soc.* **61**, 536 (1939).
- [50] J. Kollonitsch and O. Fuchs, *Nature* **176**, 1081 (1955).
- [51] P. Rittmeyer and U. Wietelmann, in: *Ullmann's Encyclopaedia of Industrial Chemistry* (Wiley-VCH, Weinheim, 2000).
- [52] H. I. Schlesinger and H. C. Brown, *J. Am. Chem. Soc.* **62**, 3429–3435 (1940).
- [53] H. C. Brown, Y. M. Choi, and S. Narasimhan, *Inorg. Chem.* **21**, 3657–3661 (1982).
- [54] H. I. Schlesinger, H. C. Brown, and E. K. Hyde, *J. Am. Chem. Soc.* **75**, 209–213 (1953).
- [55] D. Goerrig, German Patent No. 1077 644 (1958).
- [56] M. D. Banus, R. W. Bragdon, and A. A. Hinckley, *J. Am. Chem. Soc.* **76**, 3848–3849 (1954).
- [57] E. Wiberg and R. Bauer, *Z. Naturforsch.* **5B**, 397 (1950).
- [58] K. Chłopek, C. Frommen, A. Léon, O. Zabara, and M. Fichtner, *J. Mater. Chem.* **17**, 3496–3503 (2007).
- [59] P. Zanella, L. Crociani, N. Masciocchi, and G. Giunchi, *Inorg. Chem.* **46**, 9039–9041 (2007).
- [60] V. I. Mikheeva and L. V. Titov, *Zh. Neorg. Khim.* **9**, 789 (1964).
- [61] C. Suryanarayana, *Prog. Mater. Sci.* **46**, 1–184 (2001).
- [62] V. P. Balema, J. W. Wiench, M. Pruski, and V. K. Pecharsky, *Chem. Commun.* **7**, 724–725 (2002).
- [63] L. Takacs, *Prog. Mater. Sci.* **47**, 355–414 (2002).
- [64] V. P. Balema, *Mater. Matter.* **2**, 16–18 (2007).
- [65] C. Frommen, N. Aliouane, S. Deledda, J. E. Fonnelløp, H. Grove, K. Lieutenant, I. Llamas-Jansa, S. Sartori, M. H. Sørby, and B. C. Hauback, *J. Alloys Compd.* **496**, 710–716 (2010).
- [66] D. B. Ravnsbæk, Y. Filinchuk, R. Černý, M. B. Ley, D. Haase, H. J. Jakobsen, J. Skibsted, and T. R. Jensen, *Inorg. Chem.* **49**, 3801–3809 (2010).
- [67] T. Sato, K. Miwa, Y. Nakamori, K. Ohoyama, H. Li, T. Noritake, M. Aoki, S. I. Towata, and S. I. Orimo, *Phys. Rev. B* **77**, 104114 (2008).
- [68] T. Jaroń and W. Grochala, *Dalton Trans.* **39**, 160 (2010).
- [69] Y. Lee, J. Shim, and Y. Cho, *J. Phys. Chem. C* **114**, 12833–12837 (2010).
- [70] D. B. Ravnsbæk, L. H. Sørensen, Y. Filinchuk, D. Reed, D. Book, H. J. Jakobsen, F. Besenbacher, J. Skibsted, and T. R. Jensen, *Eur. J. Inorg. Chem.* **11**, 1608–1612 (2010).
- [71] T. Klassen, M. Oehring, and R. Bormann, *Acta Mater.* **45**, 3935–3948 (1997).
- [72] T. Klassen, M. Oehring, and R. Bormann, *J. Mater. Res.* **9**, 47–52 (1994).
- [73] M. Oehring, T. Klassen, and R. Bormann, *J. Mater. Res.* **8**, 2819–2829 (1993).
- [74] C. Gente, M. Oehring, and R. Bormann, *Phys. Rev. B* **48**, 13244–13252 (1993).
- [75] L. Mosegaard, B. Møller, J. Jørgensen, Y. Filinchuk, Y. Cerenius, J. C. Hanson, E. Dimasi, F. Besenbacher, and T. R. Jensen, *J. Phys. Chem. C* **112**, 1299–1303 (2008).
- [76] N. Eigen, C. Keller, M. Dornheim, T. Klassen, and R. Bormann, *Scr. Mater.* **56**, 847–851 (2007).
- [77] V. Bérubé, G. Radtke, M. Dresselhaus, and G. Chen, *Int. J. Energy J.* **31**, 637–663 (2007).
- [78] V. Gertsman and R. Birringer, *Scr. Metall. Mater.* **30**, 577–581 (1994).
- [79] B. Vigeholm, J. Kjöllér, B. Larsen, and A. Schröder Pedersen, *Int. J. Hydrogen Energy* **8**, 809–817 (1983).
- [80] L. Berlouis, E. Cabrera, E. Hall-Barientos, P. Hall, S. Dodd, S. Morris, and M. Imam, *J. Mater. Res.* **16**, 45–57 (2001).
- [81] J. Gao, P. Adelhelm, M. H. W. Verkuijlen, C. Rongeat, M. Herrich, P. J. M. van Bentum, O. Gutfleisch, A. P. M. Kentgens, K. P. de Jong, and P. E. de Jongh, *J. Phys. Chem. C* **114**, 4675–4682 (2010).
- [82] M. H. W. Verkuijlen, J. Gao, P. Adelhelm, P. J. M. van Bentum, P. E. de Jongh, and A. P. M. Kentgens, *J. Phys. Chem. C* **114**, 4683–4692 (2010).
- [83] W. Lohstroh, A. Roth, H. Hahn, and M. Fichtner, *ChemPhysChem* **11**, 789–792 (2010).
- [84] R. D. Stephens, A. F. Gross, S. L. Atta, J. J. Vajo, and F. E. Pinkerton, *Nanotechnology* **20**, 204018 (2009).
- [85] E. Dujardin, T. W. Ebbesen, H. Hiura, and K. Tanigaki, *Science* **265**, 1850 (1994).
- [86] P. G. de Gennes, *Rev. Mod. Phys.* **57**, 827–863 (1985).
- [87] A. Gutowska, L. Li, Y. Shin, C. M. Wang, X. S. Li, J. C. Linehan, R. S. Smith, B. D. Kay, B. Schmid, W. Shaw, M. Gutowski, and T. Autrey, *Angew. Chem. Int. Ed.* **44**, 3578–3582 (2005).
- [88] S. Zhang, A. F. Gross, S. L. Atta, M. Lopez, P. Liu, C. C. Ahn, J. J. Vajo, and C. M. Jensen, *Nanotechnology* **20**, 204027 (2009).
- [89] E. A. Nickels, M. O. Jones, W. I. David, S. R. Johnson, R. L. Lowton, M. Sommariva, and P. P. Edwards, *Angew. Chem. Int. Ed.* **47**, 2817–2819 (2008).
- [90] H. W. Li, S. I. Orimo, Y. Nakamori, K. Miwa, N. Ohba, S. Towata, and A. Züttel, *J. Alloys Compd.* **446/447**, 315–318 (2007).

- [91] R. Černý, N. Penin, H. Hagemann, and Y. Filinchuk, *J. Phys. Chem. C* **113**, 9003–9007 (2009).
- [92] R. Černý, N. Penin, V. d'Anna, and J. Ruziska, *Acta Mater.* **59**, 5171–5180 (2011).
- [93] R. Černý, G. Severa, D. B. Ravnsbæk, Y. Filinchuk, V. d'Anna, H. Hagemann, D. Haase, C. M. Jensen, and T. R. Jensen, *J. Phys. Chem. C* **114**, 1357–1364 (2010).
- [94] R. Černý, D. B. Ravnsbæk, G. Severa, Y. Filinchuk, V. d'Anna, H. Hagemann, D. Haase, J. Skibsted, C. M. Jensen, and T. R. Jensen, *J. Phys. Chem. C* **114**, 19540–19549 (2010).
- [95] R. Černý, K. C. Kim, N. Penin, V. d'Anna, H. Hagemann, and D. S. Sholl, *J. Phys. Chem. C* **114**, 19127–19133 (2010).
- [96] H. Hagemann, M. Longhini, J. W. Kaminski, T. A. Wesolowski, R. Černý, N. Penin, M. H. Sørby, B. C. Hauback, G. Severa, and C. M. Jensen, *J. Phys. Chem. A* **112**, 7551–7555 (2008).
- [97] Y. Filinchuk, A. V. Talyzin, H. Hagemann, V. Dmitriev, D. Chernyshov, and B. Sundqvist, *Inorg. Chem.* **49**, 5285–5292 (2010).
- [98] T. K. Maji, R. Matsuda, and S. Kitagawa, *Nature Mater.* **6**, 142–148 (2007).
- [99] Y. Filinchuk, R. Černý, and H. Hagemann, *Chem. Mater.* **21**, 925–933 (2009).
- [100] D. S. Marynick and W. N. Lipscomb, *Inorg. Chem.* **11**, 820–823 (1972).
- [101] R. W. Broach, I. S. Chuang, T. J. Marks, and J. M. Williams, *Inorg. Chem.* **22**, 1081–1084 (1983).
- [102] P. H. Bird and M. R. Churchill, *Chem. Commun. Lond.* **8**, 403 (1967).
- [103] D. B. Ravnsbæk, M. B. Ley, Y. S. Lee, H. Hagemann, V. d'Anna, Y. W. Cho, Y. Filinchuk, and T. R. Jensen, (2011) Submitted.
- [104] I. Lindemann, R. Ferrer, L. Dunsch, Y. Filinchuk, R. Černý, H. Hagemann, V. d'Anna, L. M. L. Daku, L. Schultz, and O. Gutfleisch, *Chem. Eur. J.* **16**, 8707–8712 (2010).
- [105] Y. E. Filinchuk, K. Yvon, G. P. Meisner, F. E. Pinkerton, and M. P. Balogh, *Inorg. Chem.* **45**, 1433–1435 (2006).
- [106] C. Kim, S. Hwang, R. C. Bowman, J. W. Reiter, J. A. Zan, J. G. Kulleck, H. Kabbour, E. H. Majzoub, and V. Ozolins, *J. Phys. Chem. C* **113**, 9956–9968 (2009).
- [107] R. Černý, Y. Filinchuk, H. Hagemann, and K. Yvon, *Angew. Chem. Int. Ed.* **46**, 5765–5767 (2007).
- [108] J. P. Soulie, G. Renaudin, R. Černý, and K. Yvon, *J. Alloys Compd.* **346**, 200–205 (2002).
- [109] Y. Filinchuk, D. Chernyshov, A. Nevidomskyy, and V. Dmitriev, *Angew. Chem. Int. Ed.* **47**, 529–532 (2008).
- [110] Y. Filinchuk, D. Chernyshov, and R. Černý, *J. Phys. Chem. C* **112**, 10579–10584 (2008).
- [111] D. B. Ravnsbæk, C. Frommen, D. Reed, Y. Filinchuk, M. H. Sørby, B. C. Hauback, H. J. Jakobsen, D. Book, F. Besenbacher, J. Skibsted, and T. R. Jensen, *J. Alloys Compd.* (2011). DOI: 10.1016/J.jallcom.2010.11.008.
- [112] L. Mosegaard, B. Møller, J. E. Jørgensen, U. Bösenberg, M. Dornheim, J. C. Hanson, Y. Cerenius, G. S. Walker, H. J. Jakobsen, F. Besenbacher, and T. R. Jensen, *J. Alloys Compd.* **446/447**, 301–305 (2007).
- [113] O. Friedrichs, A. Borgschulte, S. Kato, F. Buchter, R. Gremaud, A. Remhof, and A. Züttel, *Chem. Eur. J.* **15**, 5531–5534 (2009).
- [114] J. H. Her, M. Yousufuddin, W. Zhou, S. S. Jalisatgi, J. G. Kulleck, J. A. Zan, S. J. Hwang, R. C. Bowman, Jr., and T. J. Udovic, *Inorg. Chem.* **47**, 9757–9759 (2008).
- [115] O. Friedrichs, A. Remhof, S. Hwang, and A. Züttel, *Chem. Mater.* **22**, 3265–3268 (2010).
- [116] S. I. Orimo, Y. Nakamori, G. Kitahara, K. Miwa, N. Ohba, S. Towata, and A. Züttel, *J. Alloys Compd.* **404–406**, 427–430 (2005).
- [117] N. Ohba, K. Miwa, M. Aoki, T. Noritake, S. Towata, Y. Nakamori, S. I. Orimo, and A. Züttel, *Phys. Rev. B* **74**, 75110 (2006).
- [118] S. I. Orimo, Y. Nakamori, N. Ohba, K. Miwa, M. Aoki, S. I. Towata, and A. Züttel, *Appl. Phys. Lett.* **89**, 021920 (2006).
- [119] O. Friedrichs, A. Remhof, A. Borgschulte, F. Buchter, S. I. Orimo, and A. Züttel, *Phys. Chem. Chem. Phys.* **12**, 10919–10922 (2010).
- [120] J. Kostka, W. Lohstroh, M. Fichtner, and H. Hahn, *J. Phys. Chem. C* **111**, 14026–14029 (2007).
- [121] A. F. Holleman and E. Wiberg, *Inorganic Chemistry* (Academic Press, New York, 1995).
- [122] J. H. Shim, J. H. Lim, S. Rather, Y. S. Lee, D. Reed, Y. Kim, D. Book, and Y. W. Cho, *J. Phys. Chem. Lett.* **1**, 59–63 (2009).
- [123] J. W. Kim, J. H. Shim, J. P. Ahn, Y. W. Cho, J. H. Kim, and K. H. Oh, *Mater. Lett.* **62**, 2461–2464 (2008).
- [124] P. Martelli, R. Caputo, A. Remhof, P. Mauron, A. Borgschulte, and A. Züttel, *J. Phys. Chem. C* **114**, 7173–7177 (2010).
- [125] J. Urganani, F. J. Torres, M. Palumbo, and M. Baricco, *Int. J. Hydrogen Energy* **33**, 3111–3115 (2008).
- [126] D. S. Stasinevich and G. A. Egorenko, *Russ. J. Inorg. Chem.* **13**, 341–343 (1968).
- [127] G. Severa, E. Rönnebro, and C. M. Jensen, *Chem. Commun.* **46**, 421–423 (2010).
- [128] G. L. Soloveichik, Y. Gao, J. Rijssenbeek, M. Andrus, S. Kniajanski, R. C. Bowman, S. J. Hwang, and J. C. Zhao, *Int. J. Hydrogen Energy* **34**, 916–928 (2009).
- [129] T. Matsunaga, F. Buchter, P. Mauron, M. Bielman, Y. Nakamori, S. I. Orimo, N. Ohba, K. Miwa, S. Towata, and A. Züttel, *J. Alloys Compd.* **459**, 583–588 (2008).
- [130] L. George and S. K. Saxena, *Int. J. Hydrogen Energy* **35**, 5454–5470 (2010).
- [131] S. Sartori, K. D. Knudsen, Z. Zhao-Karger, E. G. Bardají, M. Fichtner, and B. C. Hauback, *Nanotechnology* **20**, 505702 (2009).
- [132] M. Fichtner, Z. Zhao-Karger, J. Hu, A. Roth, and P. Weidler, *Nanotechnology* **20**, 204029 (2009).
- [133] H. W. Li, K. Kikuchi, Y. Nakamori, N. Ohba, K. Miwa, S. Towata, and S. I. Orimo, *Acta Mater.* **56**, 1342–1347 (2008).
- [134] S. Hwang, R. C. Bowman, J. W. Reiter, J. Rijssenbeek, G. L. Soloveichik, J. Zhao, H. Kabbour, and C. C. Ahn, *J. Phys. Chem. C* **112**, 3164–3169 (2008).
- [135] H. W. Li, K. Miwa, N. Ohba, T. Fujita, T. Sato, Y. Yan, S. Towata, M. W. Chen, and S. Orimo, *Nanotechnology* **20**, 204013 (2009).
- [136] C. Pistidda, S. Garroni, F. Dolci, E. G. Bardají, A. Khandelwal, P. Nolis, M. Dornheim, R. Gosalawit, T. Jensen, Y. Cerenius, S. Suriñach, M. D. Baró, W. Lohstroh, and M. Fichtner, *J. Alloys Compd.* **508**, 212–215 (2010).

- [137] M. Aoki, K. Miwa, T. Noritake, N. Ohba, M. Matsumoto, H.-W. Li, Y. Nakamori, S. Towata, and S. I. Orimo, *Appl. Phys. A* **92**, 601–605 (2008).
- [138] K. Miwa, M. Aoki, T. Noritake, N. Ohba, Y. Nakamori, S. I. Towata, A. Züttel, and S. Orimo, *Phys. Rev. B* **74**, 155122 (2006).
- [139] Y. Yan, H. W. Li, T. Sato, N. Umeda, K. Miwa, S. I. Towata, and S. I. Orimo, *Int. J. Hydrogen Energy* **34**, 5732–5736 (2009).
- [140] Y. Filinchuk and H. Hagemann, *Eur. J. Inorg. Chem.* **20**, 3127–3133 (2008).
- [141] M. Corno, E. Pinatel, P. Ugliengo, and M. Baricco, *J. Alloys Compd.* (2011); DOI: 10.1016/j.jallcom.2010.10.005.
- [142] L. Mosegaard, B. Møller, J. E. Jørgensen, Y. Cerenius, J. C. Hanson, F. Besenbacher, H. J. Jakobsen, and T. R. Jensen, Dehydrogenation of LiBH₄ Investigated Using in Situ Synchrotron X-Ray Diffraction and MAS NMR. in: Presented at MH2006 International Symposium on Metal-Hydrogen Systems, Lahaina, HI, 1–6 October 2006.
- [143] L. H. Rude, O. Zavorotynska, L. M. Arnbjerg, D. B. Ravnsbæk, R. A. Malmkjær, H. Grove, B. C. Hauback, M. Baricco, Y. Filinchuk, F. Besenbacher, and T. R. Jensen, (2011), submitted.
- [144] L. H. Rude, E. Groppo, L. M. Arnbjerg, D. B. Ravnsbæk, R. A. Malmkjær, Y. Filinchuk, M. Baricco, F. Besenbacher, and T. R. Jensen, *J. Alloys Compd.* (2011), DOI: 10.1016/j.jallcom.2010.02.180.
- [145] H. Maekawa, M. Matsuo, H. Takamura, M. Ando, Y. Noda, T. Karahashi, and S. Orimo, *J. Am. Chem. Soc.* **131**, 894–895 (2009).
- [146] M. Matsuo, H. Takamura, H. Maekawa, H. Li, and S. I. Orimo, *Appl. Phys. Lett.* **94**, 084103 (2009).
- [147] H. Oguchi, M. Matsuo, J. S. Hummelshøj, T. Vegge, J. K. Nørskov, T. Sato, Y. Miura, H. Takamura, H. Maekawa, and S. I. Orimo, *Appl. Phys. Lett.* **94**, 141912 (2009).
- [148] A. Borgschulte, R. Gremaud, S. Kato, N. P. Stadie, A. Remhof, A. Züttel, M. Matsuo, and S. I. Orimo, *Appl. Phys. Lett.* **97**, 031916 (2010).
- [149] D. B. Ravnsbæk, L. H. Rude, and T. R. Jensen, *J. Solid State Chem.* **184**, 1858–1866 (2011).
- [150] L. H. Rude, Y. Filinchuk, M. H. Sørby, B. C. Hauback, F. Besenbacher, and T. R. Jensen, *J. Phys. Chem. C* **115**, 7768–7777 (2011).
- [151] X. Kang, P. Wang, and H. Cheng, *Scr. Mater.* **56**, 361–364 (2007).
- [152] H. W. Brinks, A. Fossdal, and B. C. Hauback, *J. Phys. Chem. C* **112**, 5658–5661 (2008).
- [153] N. Eigen, U. Bösenberg, J. Bellosta von Colbe, T. R. Jensen, Y. Cerenius, M. Dornheim, T. Klassen, and R. Bormann, *J. Alloys Compd.* **477**, 76–80 (2009).
- [154] B. C. Hauback, *Z. Kristallogr.* **223**, 636–648 (2008).
- [155] L. C. Yin, P. Wang, Z. Fang, and H. M. Cheng, *Chem. Phys. Lett.* **450**, 318–321 (2008).
- [156] G. G. Libowitz, H. F. Hayes, and T. R. P. Gibb, *J. Phys. Chem. C* **62**, 76–79 (1958).
- [157] Y. Zhang, Q. Tian, H. Chu, J. Zhang, L. Sun, J. Sun, and Z. Wen, *J. Phys. Chem. C* **113**, 21964–21969 (2009).
- [158] Y. Zhang, Q. Tian, J. Zhang, S. S. Liu, and L. X. Sun, *J. Phys. Chem. C* **113**, 18424–18430 (2009).
- [159] A. Remhof, O. Friedrichs, F. Buchter, P. Mauron, J. W. Kim, K. H. Oh, A. Buchsteiner, D. Wallacher, and A. Züttel, *J. Alloys Compd.* **484**, 654–659 (2009).
- [160] J. W. Kim, O. Friedrichs, J. P. Ahn, D. H. Kim, S. C. Kim, A. Remhof, H. S. Chung, J. Lee, J. H. Shim, Y. W. Cho, A. Züttel, and K. H. Oh, *Scr. Mater.* **60**, 1089–1092 (2009).
- [161] O. Friedrichs, J. W. Kim, A. Remhof, F. Buchter, A. Borgschulte, D. Wallacher, Y. W. Cho, M. Fichtner, K. H. Oh, and A. Züttel, *Phys. Chem. Chem. Phys.* **11**, 1515–1520 (2009).
- [162] D. B. Ravnsbæk and T. R. Jensen, *J. Phys. Chem. Solids* **71**, 1144–1149 (2010).
- [163] G. Barkhordarian, T. Klassen, M. Dornheim, and R. Bormann, *J. Alloys Compd.* **440**, L18–L21 (2007).
- [164] P. Chen, Z. Xiong, J. Luo, J. Lin, and K. L. Tan, *Nature* **420**, 302–304 (2002).
- [165] Z. Xiong, J. Hu, G. Wu, P. Chen, W. Luo, K. Gross, and J. Wang, *J. Alloys Compd.* **398**, 235–239 (2005).
- [166] G. Barkhordarian, T. Klassen, and R. Bormann, U.S. Patent No. DE102004/061286 (2004).
- [167] J. J. Vajo, F. O. Mertens, S. L. Skeith, and M. P. Balogh, U.S. Patent No. WO2005/097671 A2 (2004).
- [168] J. H. Lim, J. H. Shim, Y. S. Lee, J. Y. Suh, Y. W. Cho, and J. Lee, *Int. J. Hydrogen Energy* **35**, 6578–6582 (2010).
- [169] H. Hagemann, V. D’Anna, J. Rapin, R. Černý, Y. Filinchuk, K. C. Kim, D. S. Sholl, and S. F. Parker, *J. Alloys Compd.* (2010). DOI:10.1016/J.jallcom.2010.10.068.
- [170] G. Barkhordarian, T. R. Jensen, S. Doppiu, U. Bösenberg, A. Borgschulte, R. Gremaud, Y. Cerenius, M. Dornheim, T. Klassen, and R. Bormann, *J. Phys. Chem. C* **112**, 2743–2749 (2008).
- [171] J. J. Vajo and G. L. Olson, *Scr. Mater.* **56**, 829–834 (2007).
- [172] J. Purewal, S. J. Hwang, J. Bowman, E. Rönnebro, B. Fultz, and C. Ahn, *J. Phys. Chem. C* **112**, 8481–8485 (2008).
- [173] S. V. Alapati, J. K. Johnson, and D. S. Sholl, *J. Phys. Chem. B* **110**, 8769–8776 (2006).
- [174] F. E. Pinkerton, M. S. Meyer, G. P. Meisner, M. P. Balogh, and J. J. Vajo, *J. Phys. Chem. C* **111**, 12881–12885 (2007).
- [175] J. Yang, A. Sudik, and C. Wolverton, *J. Phys. Chem. C* **111**, 19134–19140 (2007).
- [176] S. A. Jin, Y. S. Lee, J. H. Shim, and Y. W. Cho, *J. Phys. Chem. C* **112**, 9520–9524 (2008).
- [177] P. Mauron, M. Biemann, A. Remhof, A. Züttel, J. H. Shim, and Y. W. Cho, *J. Phys. Chem. C* **114**, 16801–16805 (2010).
- [178] O. Friedrichs, F. Buchter, A. Borgschulte, A. Remhof, C. N. Zwicky, P. Mauron, M. Biemann, and A. Züttel, *Acta Mater.* **56**, 949–954 (2008).
- [179] Y. Kim, D. Reed, Y. Lee, J. Shim, H. N. Han, D. Book, and Y. W. Cho, *J. Alloys Compd.* **492**, 597–600 (2009).
- [180] U. Bösenberg, D. B. Ravnsbæk, H. Hagemann, V. D’Anna, C. B. Minella, C. Pistidda, W. van Beek, T. R. Jensen, R. Bormann, and M. Dornheim, *J. Phys. Chem. C* **114**, 15212–15217 (2010).
- [181] X. B. Yu, D. M. Grant, and G. S. Walker, *Chem. Commun.* **37**, 3906–3908 (2006).
- [182] V. Ozolins, E. H. Majzoub, and C. Wolverton, *J. Am. Chem. Soc.* **131**, 230–237 (2008).
- [183] U. Bösenberg, U. Vainio, P. K. Pranzas, J. M. Colbe, G. Goerigk, E. Welter, M. Dornheim, A. Schreyer, and R. Bormann, *Nanotechnology* **20**, 204003 (2009).
- [184] T. E. C. Price, D. M. Grant, I. Telegen, X. B. Yu, and G. S. Walker, *J. Alloys Compd.* **472**, 559–564 (2009).
- [185] T. E. Price, D. M. Grant, V. Legrand, and G. S. Walker, *Int. J. Hydrogen Energy* **35**, 4154–4161 (2010).

- [186] J. F. Mao, Z. Wu, T. J. Chen, B. C. Weng, N. X. Xu, T. S. Huang, Z. P. Guo, H. K. Liu, D. M. Grant, G. S. Walker, and X. B. Yu, *J. Phys. Chem. C* **111**, 12945–12948 (2007).
- [187] T. Nakagawa, T. Ichikawa, N. Hanada, Y. Kojima, and H. Fujii, *J. Alloys Compd.* **446**, 306–309 (2007).
- [188] J. Z. Hu, J. H. Kwak, Z. Yang, X. Wan, and L. L. Shaw, *Appl. Phys. Lett.* **94**, 141905 (2009).
- [189] L. Zeng, H. Miyaoka, T. Ichikawa, and Y. Kojima, *J. Phys. Chem. C* **114**, 13132–13135 (2010).
- [190] J. J. Vajo, W. Li, and P. Liu, *Chem. Commun.* **46**, 6687–6689 (2010).
- [191] G. S. Walker, D. M. Grant, T. C. Price, X. Yu, and V. Legrand, *J. Power Sources* **194**, 1128–1134 (2009).
- [192] T. R. Jensen, T. K. Nielsen, Y. Filinchuk, J. E. Jørgensen, Y. Cerenius, E. M. Gray, and C. J. Webb, *J. Appl. Crystallogr.* **43**, 1456–1463 (2010).
- [193] A. Y. Ignatov, J. Graetz, S. Chaudhuri, T. T. Salguero, J. J. Vajo, M. S. Meyer, F. E. Pinkerton, and T. A. Tyson, *X-Ray Absorption Fine Structure–XAFS 13*, AIP Conf. Proc. **882**, 642–644 (2007).
- [194] E. Deprez, M. A. Muñoz-Márquez, M. A. Roldán, C. Prestipino, F. J. Palomares, C. B. Minella, U. Bösenberg, M. Dornheim, R. Bormann, and A. Fernández, *J. Phys. Chem. C* **114**, 3309–3317 (2010).
- [195] E. Deprez, A. Justo, T. C. Rojas, C. López-Cartés, C. Bonatto Minella, U. Bösenberg, M. Dornheim, R. Bormann, and A. Fernández, *Acta Mater.* **58**, 5683–5694 (2010).
- [196] J. Graetz, S. Chaudhuri, T. T. Salguero, J. J. Vajo, M. S. Meyer, and F. E. Pinkerton, *Nanotechnology* **20**, 204007 (2009).
- [197] Y. Kim, D. Reed, Y. Lee, J. Y. Lee, J. Shim, D. Book, and Y. W. Cho, *J. Phys. Chem. C* **113**, 5865–5871 (2009).
- [198] M. Gonzalez-Silveira, R. Gremaud, H. Schreuders, M. J. Setten, E. Batyrev, A. Rougier, L. Dupont, E. G. Bardají, W. Lohstroh, and B. Dam, *J. Phys. Chem. C* **114**, 13895–13901 (2010).
- [199] C. Bonatto-Minella, S. Garroni, C. Pistidda, R. Gosalawit-Utke, G. Barkhordarian, C. Rongeat, I. Lindemann, O. Gutfleisch, T. R. Jensen, Y. Cerenius, J. Christensen, M. D. Baró, R. Bormann, T. Klassen, and M. Dornheim, *J. Phys. Chem. C* **115**, 2497–2504 (2011).
- [200] V. Berube, G. Chen, and M. S. Dresselhaus, *Int. J. Hydrogen Energy* **33**, 4122–4131 (2008).
- [201] L. Zaluski, A. Zaluska, and J. O. Ström-Olsen, *J. Alloys Compd.* **253**, 70–79 (1997).
- [202] X. Yao, Z. H. Zhu, H. M. Cheng, and G. Q. Lu, *J. Mater. Res.* **23**, 336–340 (2008).
- [203] R. Kirchheim, T. Mütschele, W. Kieninger, H. Gleiter, R. Birringer, and T. D. Koble, *Mater. Sci. Eng.* **99**, 457–462 (1988).
- [204] S. Cheung, W. Q. Deng, A. C. van Duin, and W. A. Goddard, III, *J. Phys. Chem. A* **109**, 851–859 (2005).
- [205] J. J. Liang, *Appl. Phys. A* **80**, 173–178 (2005).
- [206] R. W. Wagemans, J. H. van Lenthe, P. E. de Jongh, A. J. van Dillen, and K. P. de Jong, *J. Am. Chem. Soc.* **127**, 16675–16680 (2005).
- [207] X. D. Yao and G. Lu, *Chin. Sci. Bull.* **53**, 2421–2431 (2008).
- [208] A. F. Gross, J. J. Vajo, S. L. Van Atta, and G. L. Olson, *J. Phys. Chem. C* **112**, 5651–5657 (2008).
- [209] A. F. Gross, C. C. Ahn, S. L. Atta, P. Liu, and J. J. Vajo, *Nanotechnology* **20**, 204005 (2009).
- [210] R. Bogerd, P. Adelhelm, J. H. Meeldijk, K. P. Jong, and P. E. Jongh, *Nanotechnology* **20**, 204019 (2009).
- [211] P. E. Jongh, R. W. Wagemans, T. M. Eggenhuisen, B. S. Dauvillier, P. B. Radstake, J. D. Meeldijk, J. W. Geus, and K. P. Jong, *Chem. Mater.* **19**, 6052–6057 (2007).
- [212] A. Feaver, S. Sepehri, P. Shamberger, A. Stowe, T. Autrey, and G. Cao, *J. Phys. Chem. B* **111**, 7469–7472 (2007).
- [213] G. Wolf, J. Baumann, F. Baitalow, and F. P. Hoffmann, *Thermochim. Acta* **343**, 19–25 (2000).
- [214] C. Rongeat, I. Llamas Jansa, S. Oswald, L. Schultz, and O. Gutfleisch, *Acta Mater.* **57**, 5563–5570 (2009).
- [215] J. Wang, A. D. Ebner, T. Prozorov, R. Zidan, and J. A. Ritter, *J. Alloys Compd.* **395**, 252–262 (2005).
- [216] K. J. Gross, G. J. Thomas, and C. M. Jensen, *J. Alloys Compd.* **330**, 683–690 (2002).
- [217] T. Mueller and G. Ceder, *ACS Nano* **4**, 5647–5656 (2010).
- [218] T. K. Nielsen, M. Polanski, D. Zasada, P. Javadian, F. Besenbacher, J. Bystrzycki, J. Skibsted, and T. R. Jensen, *ACS Nano* **5**, 4056–4064 (2011).
- [219] V. Sit, R. A. Geanangel, and W. W. Wendlandt, *Thermochim. Acta* **113**, 379–382 (1987).
- [220] L. Li, X. Yao, C. H. Sun, A. J. Du, L. N. Cheng, Z. H. Zhu, C. Z. Yu, J. Zou, S. C. Smith, P. Wang, H. M. Cheng, R. L. Frost, and G. Q. M. Lu, *Adv. Funct. Mater.* **19**, 265–271 (2009).
- [221] S. Sepehri, A. Feaver, W. J. Shaw, C. J. Howard, Q. Zhang, T. Autrey, and G. Cao, *J. Phys. Chem. B* **111**, 14285–14289 (2007).